Science of the Total Environment 895 (2023) 165059

Contents lists available at ScienceDirect

Science of the Total Environment

journal homepage: www.elsevier.com/locate/scitotenv

# Experimental and in silico evaluations of the possible molecular interaction between airborne particulate matter and SARS-CoV-2

Alice Romeo [a], Roberto Pellegrini [a,b], Maurizio Gualtieri [c,d], Barbara Benassi [b], Massimo Santoro [b], Federico Iacovelli [a], Milena Stracquadanio [c], Mattia Falconi [a], Carmela Marino [b], Gabriele Zanini [c], Caterina Arcangeli [b,*]

[a] Department of Biology, University of Rome Tor Vergata, Via della Ricerca Scientifica 1, 00133 Rome, Italy
[b] Division of Health Protection Technologies, Italian National Agency for New Technologies, Energy and Sustainable Development (ENEA), 00123 Rome, Italy
[c] Division of Models and Technologies for Risks Reduction, Italian National Agency for New Technologies, Energy and Sustainable Development (ENEA), 40129 Bologna, Italy
[d] Department of Earth and Environmental Sciences, Piazza della Scienza 1, University of Milano-Bicocca, Milano

## HIGHLIGHTS

- Positive correlation between the elemental carbon content of PM and SARS-CoV-2 mRNA
- First structural model of airborne PM by HPC Molecular Dynamics Simulations
- Plausible molecular mechanism of PM and SARS-CoV-2 association
- Crucial role of the Spike protein's glycans during the attachment process to the PM

## GRAPHICAL ABSTRACT

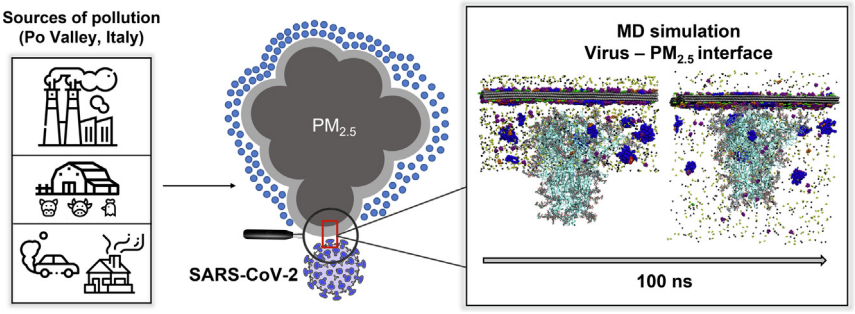


## ARTICLE INFO

Editor: Hai Guo

*Keywords:*
Classical molecular dynamics simulation
$PM_{2.5}$
SARS-CoV-2
COVID-19 pandemic

## ABSTRACT

During the early stage of the COVID-19 pandemic (winter 2020), the northern part of Italy has been significantly affected by viral infection compared to the rest of the country leading the scientific community to hypothesize that airborne particulate matter (PM) could act as a carrier for the SARS-CoV-2. To address this controversial issue, we first verified and demonstrated the presence of SARS-CoV-2 RNA genome on $PM_{2.5}$ samples, collected in the city of Bologna (Northern Italy) in winter 2021. Then, we employed classical molecular dynamics (MD) simulations to investigate the possible recognition mechanism(s) between a newly modelled $PM_{2.5}$ fragment and the SARS-CoV-2 Spike protein. The potential molecular interaction highlighted by MD simulations suggests that the glycans covering the upper Spike protein regions would mediate the direct contact with the $PM_{2.5}$ carbon core surface, while a cloud of organic and inorganic $PM_{2.5}$ components surround the glycoprotein with a network of non-bonded interactions resulting in up to 4769 total contacts. Moreover, a binding free energy of $-207.2 \pm 3.9$ kcal/mol was calculated for the PM-Spike interface through the MM/GBSA method, and structural analyses also suggested that PM attachment does not alter the protein conformational dynamics. Although the association between the PM and SARS-CoV-2 appears plausible, this simulation does not assess whether these established interactions are sufficiently stable to carry the virus in the atmosphere, or whether the virion retains its infectiousness after the transport. While these key aspects should be

*Abbreviations:* PM, Particulate Matter; $PM_{2.5}$, fine Particulate Matter; HPC, High Performance Computing; MD, Molecular Dynamics; N, viral Nucleocapsid protein; ORF-1a/b, Viral Open Reading Frame 1 ab; $PM_{10}$, coarse Particulate Matter; PAHs, Polycyclic Aromatic Hydrocarbons; EC, Elemental Carbon; OC, Organic Carbon; S, viral Spike protein; RBD, Receptor Binding Domain; RT-PCR, Reverse Trancription- Polimerase Chain Reaction; NTD, N-Terminal Domain; SOA, Secondary Organic Aerosol; SIA, Secondary Inorganic Aerosol; BaP, Benzo[*a*]Pyrene; LVG, Levoglucosan; PTX, Phthalic acid; PLX, Palmitic acid; OXC, Oxalic acid; VdW, Van der Waals; ACE2, Angiotensin-Converting Enzyme 2.

* Corresponding author.
*E-mail address:* caterina.arcangeli@enea.it (C. Arcangeli).

http://dx.doi.org/10.1016/j.scitotenv.2023.165059
Received 20 January 2023; Received in revised form 31 May 2023; Accepted 19 June 2023
Available online 21 June 2023

verified by further experimental analyses, for the first time, this pioneering study gains insights into the molecular interactions between PM and SARS-CoV-2 Spike protein and will support further research aiming at clarifying the possible relationship between PM abundance and the airborne diffusion of viruses.

## 1. Introduction

During the early stage (winter 2020) of the COVID-19 pandemic, the Northern part of Italy has been significantly affected by the viral infection and its related diseases' outcome if compared to the rest of the country. The Lombardia region and, in general, the whole Po Valley (Northern Italy) were the geographical areas reporting the most intense and dramatic COVID-19 outbreaks. This evidence led the scientific community to hypothesize a strict relationship between the acute virus spread and the high concentrations of the airborne particulate matter (PM) (Nor et al., 2021). In fact, the Po Valley is among the most polluted areas in Europe (EEA, 2022) and, in winter, the concentrations of coarse ($PM_{10}$) and fine PM ($PM_{2.5}$) exceed the EU limit values. Despite the bulk of studies, supporting the hypothesis of particle pollution as potential carrier of SARS-CoV-2, is growing rapidly (Al Huraimel et al., 2020; Anand et al., 2021; Barakat et al., 2020; Belosi et al., 2021; Bontempi, 2020; Chung et al., 2022; Coccia, 2020; Comunian et al., 2020; Domingo and Rovira, 2020; Kayalar et al., 2021; Kumar et al., 2021; Maleki et al., 2021; Martelletti and Martelletti, 2020; Nor et al., 2021; Sanità di Toppi et al., 2020; Setti et al., 2020a, 2020b, 2020c, 2020d; Shao et al., 2021; Tang et al., 2020; Tung et al., 2021; Wang et al., 2020) this hypothesis still remains controversial and not unequivocally demonstrated.

In search of solid proofs of evidence supporting the possible air pollution-linked transmission for SARS-CoV-2, different groups focused on the presence of viral genetic material (RNA) in PM filters collected in polluted areas, where COVID-19 outbreaks were increasing. Setti and colleagues first identified the SARS-CoV-2 genome fragments on $PM_{10}$ filters collected in Bergamo (Northern Italy), an area characterized by high concentrations of particulate matter and high prevalence of COVID-19 cases if compared to the rest of Italy (Setti et al., 2020c). This genome-based approach has subsequently led to controversial results, as the detection of viral RNA in PM samples has been proven in outdoor PM samples collected in other urban areas such as in Venice (Pivato et al., 2022) and in Turkish cities (Kayalar et al., 2021), whereas no traces of SARS-CoV-2 genome were identified in outdoor PM samples carried out in areas, with local high COVID prevalence, located in both Spain (Linillos-Pradillo et al., 2021) and Italy (Padua, Venice and Lecce) (Pivato et al., 2021; Chirizzi et al., 2021). Recent literature identifies in the different methodologies applied to collect and store PM filters samples, the key determinants responsible for such inconsistency (Pivato et al., 2022; Licen et al., 2022). This makes the biological significance of the SARS-CoV-2 genome presence on PM filters still an open question and highlights the need for applying alternative and/or complementary experimental strategies to address this issue.

To this aim, we run an integrated approach, based on the characterization of the presence of SARS-CoV-2 genome on $PM_{2.5}$ quartz filters (characterized for their content in elemental (EC) and organic (OC) carbon) collected in the area of Bologna (Northern Italy) in winter 2021, combined with a *in silico* analysis of the interaction between the virus surface and a model of the EC core of fine PM. This approach has the ambition to evaluate, for the first time, the occurrence and the plausibility of the key initiating event, i.e. the actual molecular PM-virus interaction. The $PM_{2.5}$-virus interface was restricted to a fraction of $PM_{2.5}$ (a portion of the surface with few organic and inorganic molecules) and the Spike (S) protein of SARS-CoV-2. The molecular model of the $PM_{2.5}$ was constructed starting from a graphene-based surface and a mixture of organic and inorganic compounds typically representing the $PM_{2.5}$ samples collected in the Po Valley (Bologna area) during winter campaigns (Tositti et al., 2014; Pietrogrande et al., 2013). Classical molecular dynamics (MD) simulations were carried out to analyze the PM formation. The final $PM_{2.5}$ model was subsequently simulated in the presence of a model of the SARS-CoV-2 S glycoprotein, inserted in a membrane, representing a part of the envelope membrane. The main results of this study reside in the finding of a high and positive correlation between the number of SARS-CoV-2 mRNA and EC-enriched fine PM samples and in the achievement, for the first time, of a fine PM structural model and an early characterization of the PM-virus interface, through molecular modeling and MD simulations. Although preliminary, the acquired results provide new information on the structure and driving forces behind PM formation and to understand the molecular interactions between PM and viruses. The pioneering approach of this work could support further studies aimed at elucidating the relationship between the PM composition and viruses' airborne spread.

## 2. Materials and methods

### 2.1. Particulate matter ($PM_{2.5}$) filters collection

In order to detect the airborne SARS-CoV-2, $PM_{2.5}$ has been sampled for 24 h on quartz fiber filters (Pall 2500-QUAT-UP diameter 47 mm, Supplementary materials) with a retention efficiency higher than 99.95 % for particles with an aerodynamic diameter of 0.3 μm, using a low-volume sampler at a nominal flow of 2.3 $m^3\ h^{-1}$ (European standard EN 12341:2014). Fifteen daily samples were collected over the period January 19th – February 6th (2021) at the sampling site of ENEA Bologna (44°31′30″, 63 N; 11°20′40″, 92 E). Bologna area was selected as is one of the biggest cities in the Po valley and one of the most polluted areas in Europe, representing therefore a good candidate to study association between air pollution and emission sources. During the second wave of COVID-19 (winter 2021), when the restrictions for workers were in part reduced, a sampling campaign to was started to evaluate the association between COVID-19 control strategies and air pollution quality. The filters (N = 15) were numbered with the acronym BO-PULVB (1 to 15) and identified with the collection date (month/day/year). At the end of each daily sampling, filters were recovered and removed from the filter holders under a clean chemical hood in a clean plastic Petri dish. Personnel involved in filters loading and unloading were always wearing FFP2 masks and gloves to avoid any direct contact with the filters and filter holders. Just after removal from the filter holders, the filters were then sealed, wrapped in aluminium foil and directly placed at −20 °C until further use for subsequent molecular analyses. All the plastic and the consumable used for the filters were routinely washed with ethanol 70 % and milliQ water. Chemical analysis of elemental carbon (EC) was performed nearby the site of sampling (44°31′29″, 00 N, 11°20′27″0.00 E) with a thermo-optic EC/OC analyzer (Model-4 Semi-Continuous OC-EC Field Analyzer—Sunset Laboratory Inc., Sunset Laboratory Inc. Tigard, OR, USA), the hourly data were then mediated over the 24 h corresponding to the sampled filters, more details on the sampling campaign of the EC analysis are available in Costabile et al. (2022).

### 2.2. RNA extraction and SARS-CoV-2 detection

Viral RNA extraction from the quartz fiber filters was performed by using Trizol® reagent (Thermo Fisher, USA) and Quick-RNA Miniprep Kit (Zymo Research, USA), with a modified protocol specifically optimized to increase the integrity and yield of the extracted RNA. Briefly, each filter was cut in four parts and placed inside a 2 ml centrifuge tube containing 1 ml of Trizol® reagent (Thermo Fisher, USA) followed by vortexing for 10 min at room temperature to release viral particles attached to the membrane. Afterwards, 1 volume of ethanol (95–100 %) (1:1) was added to each tube and shaken vigorously for 15 s. The supernatant, containing the

viral RNA, was transferred into Zymo-Spin™ IIICG Column step 2 of Quick-RNA Miniprep Kit following the manufacturer's instructions until the elution step in 60 μl of the DNase/RNase-Free water. Total RNA was quantified by fiber optic Nanodrop ND-1000 spectrophotometer (ThermoFisher Scientific, USA) and stored frozen at −80 °C for further PCR analysis.

Reverse Transcription-PCR (RT-PCR) for the amplification and detection of the SARS-CoV-2 viral genome was carried out in the Eco Real-Time PCR System (Illumina, USA) using qPCRBIO Probe 1-Step Virus Detect kit (PCR BIOSYSTEMS, USA), optimized and validated for sensitive and qualitative detection of SARS-CoV-2 genomic RNA. The commercial kit provides all the reagents required for the one-step RT-PCR reaction, except for specific primers and probes to detect SARS-CoV-2. For viral detection, we selected the TaqMan 2019-nCoV Assay Kit v1 (Thermo Fisher, USA) that contains a set of primers and probes to amplify three different SARS-CoV-2 genes, namely the *Open reading frame 1 ab* (*ORF-1a/b*), *Spike (S) protein*, and *Nucleocapsid (N) protein* (Fig. 1a).

For each sample, 5 μl of extracted RNA were added to 14 μl of qPCRBIO Probe 1-Step Virus Detect master mix containing primers and probes (TaqMan 2019-nCoV Assay Kit v1) according to kit instructions. In each run, 1 μl of the 2019-nCoV Control v1 (Thermo Fisher, USA) (20 μl as final volume) was added as a positive control to verify the assay performance and to help with troubleshooting. The interpretation of the results was done by applying a value ≤40 as cycle threshold (CT). We considered as "positive" those $PM_{2.5}$ quartz filter samples showing amplification in at least one out of the three SARS-CoV-2 genes. Unlike the criteria reported in de la Fuente et al. (2022), we have chosen to apply these criteria for the following reasons: i) the sampling has not been carried out for clinical diagnostic purposes or for cells treatment with SARS-CoV-2/PM such as reported in de la Fuente et al. (2022); ii) the nature of the sample (detection of SARS-CoV-2 RNA on $PM_{2.5}$ quartz filter); iii) the possible occurrence of RNA genome fragmentation, due to the prolonged storage at −80 °C for months before undergoing molecular genetic analyses (as a consequence of the Italian pandemic lockdown).

### 2.3. Modeling and simulation of a $PM_{2.5}$ fragment

A simplified structural model of a $PM_{2.5}$ portion was built by including representative components of a typical secondary organic (SOA) and secondary inorganic (SIA) aerosol of the Po Valley areas collected during the "air pollution samplings" carried out by the ENEA Laboratory of Atmospheric Pollution in winter 2019. These data showed that the SIA constituted the predominant component of $PM_{2.5}$ fine particles (52 % of the total mass), while the ratio of SOA components was 1:30:30:10:20 for polycyclic aromatic hydrocarbons (PAHs), carbohydrates, alkaloid acids, aromatic acids and aliphatic acids, respectively.

Atomistic structures of selected individual compounds, representative of the listed chemical classes, were obtained from the PubChem database (Kim et al., 2021) (Table 1). The black carbon core of a typical $PM_{2.5}$ was simplified by building a 3-layers sheet of graphene with dimensions of 240 × 240 × 10 Å. This structure has been modelled using the CHARMM-GUI web interface (Jo et al., 2008) and parametrized using the CHARMM force field. CHARMM parameters for the $PM_{2.5}$ organic compounds were generated using the CGenFF program (https://cgenff.umaryland.edu) and the CHARMM general force field (Vanommeslaeghe et al., 2010). Parameters for ammonium were already included in the CHARMM force field, while those of nitrate were obtained from the literature (Richards et al., 2012). A final $PM_{2.5}$ model has been assembled using the Packmol program (Martínez et al., 2009), randomly inserting all benzo [*a*]pyrene (BaP), levoglucosan (LVG), palmitic acid (PLX), phthalic acid (PTX), oxalic acid (OXC), ammonium ($NH_4^+$) and nitrate ($NO_3^-$) molecules, facing one side of the graphene surface. The final system was solvated through the VMD software (Humphrey et al., 1996) in a 240 × 240 × 163 Å box of TIP3P water molecules (Jorgensen et al., 1983). The water molecules were added to the system to mimic the typical Po valley winter atmospheric relative humidity (that during the days of sampling was usually over 80 %, with peaks at 97 % and minimum values at 46 %, Costabile et al. (2022)). This system was then used as an input structure for a 190 ns long classical MD simulation performed using the NAMD

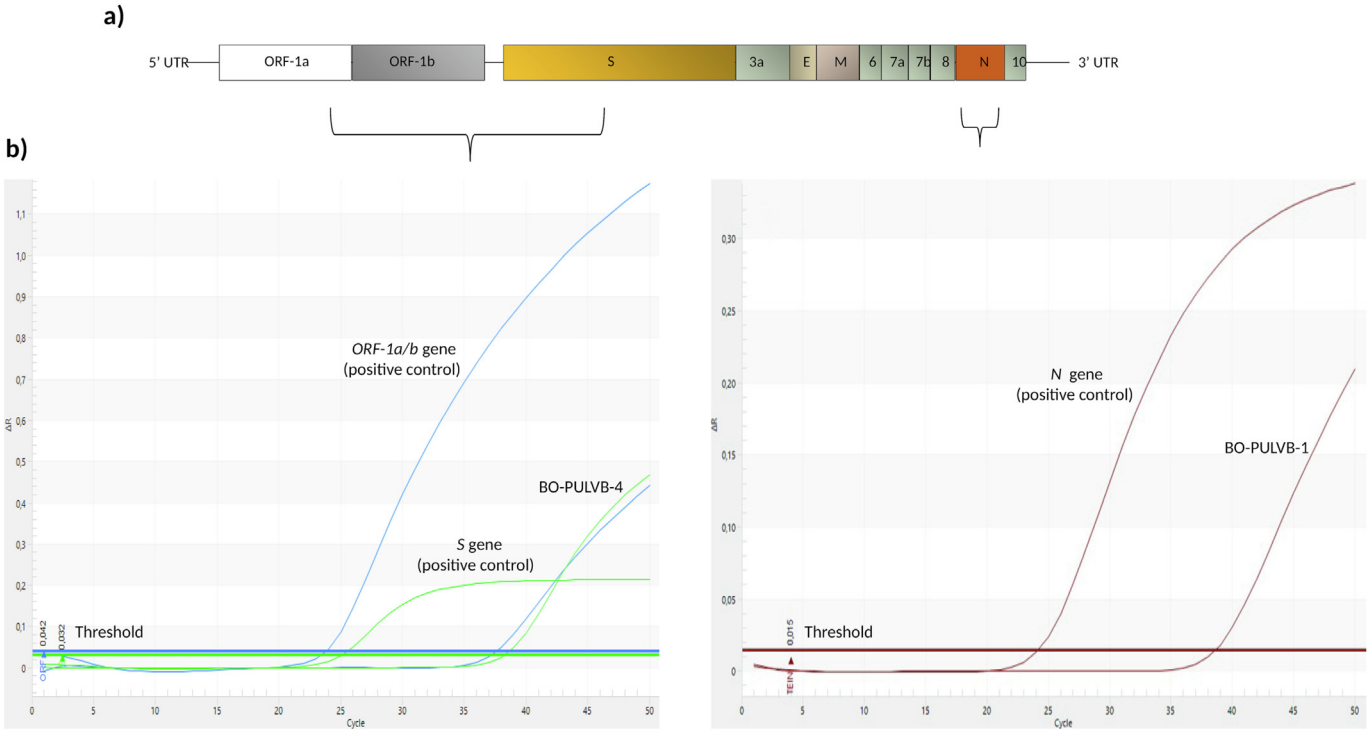


**Fig. 1.** a) Genomic structure of the SARS-CoV-2 RNA, including two open reading frames (indicated as ORF-1a and ORF-1b), Spike (S) protein, envelope (E) protein, membrane (M) protein, nucleocapsid (N) protein and other accessory proteins (indicated as numbers. b) Representative amplification plot of *ORF-1a/b*, *S* and *N* genes of positive controls, 2019-nCoV Control v1 kit, (Thermo Fisher, USA) and of two selected Bologna filter samples (Table1).

**Table 1**
The chemical composition of $PM_{2.5}$ and the representative molecules chosen for building the model. For each molecule the Pubchem CID, the abbreviation and the number of molecules used in the structural model is reported.

| Chemical composition | Representative molecule | Pubchem CID | Abbreviation | Number of molecules |
|---|---|---|---|---|
| **Secondary Organic Aerosol (SOA)** | | | | |
| PAHs class | Benzo[*a*]pyrene | 2336 | BaP | 5 |
| carbohydrate class | Levoglucosan | 2724705 | LVG | 150 |
| alkaloid acid class | Palmitic acid | 985 | PLX | 100 |
| aromatic acid class | Phthalic acid | 1017 | PTX | 50 |
| aliphatic acid class | Oxalic acid | 971 | OXC | 100 |
| **Secondary Inorganic Aerosol (SIA)** | | | | |
| Ammonium ion | $NH_4^+$ | 223 | NH4 | 493 |
| Nitrate ion | $NO_3^-$ | 943 | NO3 | 493 |

2.13 program (Phillips et al., 2005), running on the ENEA CRESCO6 HPC cluster (Iannone et al., 2019). To optimize the initial system geometry, six sequential minimization stages, including 2000 steps each, have been performed employing the conjugate gradient method. An initial constraint of 5.0 kcal/mol was applied to each atom, then halved at each subsequent minimization, and removed in the final stage. The minimized system was thermalized in a canonical (NVT) ensemble, using a timestep of 1.0 fs, gradually increasing the temperature from 0 to 300 K every 30 ps using Langevin dynamics (Goga et al., 2012). Then, the system was simulated in an anisotropic isobaric-isothermal (NPT) ensemble at a constant temperature of 300 K, fixing the pressure at 1.0 atm using the Nosè-Hoover Langevin piston method (Feller et al., 1995; Martyna et al., 1994). Electrostatic interactions were calculated using the Particle-Mesh Ewald method (Darden et al., 1993), while cut-off for short-range interactions was set to 12.0 Å. After the equilibration phase the system was stabilized within the selected simulation ensemble and, in order to obtain a more efficient sampling and to decrease the computational cost of simulations, the timestep was increased to 2.0 fs. A total of 190 ns of production dynamics were performed in which the system coordinates were saved every 1000 steps.

### 2.4. Modeling and simulation of the $PM_{2.5}$ - SARS-CoV-2 interface

A simplified model of a $PM_{2.5}$-virus interface was assembled by including a representative structure of the $PM_{2.5}$ fragment and a complete model of the glycosylated SARS-CoV-2 S protein, inserted in a membrane mimicking the viral envelope (Woo et al., 2020). The reason for selecting the Spike glycoprotein relies on the fact that it is the main external protein protruding from the virus envelope, and thus can likely interact with the $PM_{2.5}$ carbon core.

The $PM_{2.5}$ structure was the final frame of the 190 ns simulation previously described, including both the PM components stratified on the graphene sheet and those still fluctuating around the carbon core. The S glycoprotein structure was obtained from a preceding equilibrated trajectory (Romeo et al., 2022), which was performed starting from a complete model of the protein available in the CHARMM-GUI COVID 19 archive (http://www.charmm-gui.org/?doc=archive&lib=covid19). This model is based on a cryo-EM structure (Walls et al., 2020), in which the protein is in prefusion conformation, with its receptor binding domains (RBDs) in closed configuration (RBD down). The missing residues and the 22 N-linked and 1 O-linked glycans, whose composition includes *N*-acetylhexosamine, hexose, deoxyhexose, and neuraminic acid, have been modelled and made available by Woo et al. (2020).

The S protein and $PM_{2.5}$ models were approached using the VMD software (Humphrey et al., 1996) mimicking an initial interaction between the two interfaces, with the long axis of the Spike oriented perpendicular to the graphene surface. Superpositions occurring between the protein surface and surrounding compounds fluctuating in the solvent were manually fixed. The assembled system was parametrized using the CHARMM force field and then inserted in a box of TIP3P water molecules (Jorgensen et al., 1983) neutralized with 236 $K^+$ ions. The final system generated included a total of about 2.48 million atoms. Considering the enormous computational cost and time needed to simulate such a large system, the size of the simulation box was reduced by removing the protein stalk and transmembrane segments (residues 1148-1273), and consequently also the viral membrane. This new reduced system was solvated again with TIP3P water molecules and neutralized with 12 $K^+$ ions, finally including a total of 1.589.154 atoms in a 247.6 × 248.3 × 275.0 Å simulation box. This system was used as input for a 100 ns classical MD simulation, carried out as described in the previous section, using the NAMD 2.13 program (Phillips et al., 2005) on the ENEA CRESCO6 HPC cluster (Iannone et al., 2019).

### 2.5. Analysis of the MD trajectories

The trajectories have been analyzed using the GROMACS 2019 analysis tool (Abraham et al., 2015), which provides a widely documented and comprehensive set of simulation analysis modules. To exploit GROMACS features, NAMD output trajectories in *dcd* format have been converted into the GROMACS-compatible *xtc* format, using *trjconv* module of GROMACS. The root mean square deviations (RMSD) and the root mean square fluctuations (RMSF) were computed by using *rms* and *rmsf* modules, respectively. The *gyrate* module was used to compute the radius of gyration on the S protein Cα atoms. Tilt angle of the S protein was calculated using the *gangle* module, in which the vector used to calculate the angle, and identifying S orientation with respect to the z-axis normal, was defined between the Cα atoms of residues G910 and Y508 of the three protein monomers. The *mindist* module was used to analyze the minimum distance between the centers of mass of each $PM_{2.5}$ component and the graphene. The minimum distance between the residues and the glycans of the S protein and the graphene was also computed. The mean-square displacement (MSD) analysis was calculated through the *msd* module. This analysis was used to monitor the mobility of individual system components, to understand if a molecule can diffuse freely in the solvent or if its movements are limited by some constraints. In the simulation of the $PM_{2.5}$ model, the constraints can be represented by molecules' interaction with graphene or by the formation of aggregates. For each compound, diffusion coefficients ($D_{coeff}$) were calculated from the MSD through linear regression using GROMACS, averaging values at simulation intervals of 20 ns to observe the evolution of molecules' motion during the 190 ns trajectory.

Further analyses have been performed using different VMD (Humphrey et al., 1996) analysis plugins. An in-house Tcl script in VMD was employed to calculate the number of organic and inorganic molecules in contact with the graphene during the simulation time. The distance threshold for identifying a contact was set to 0.4 nm to also include short-range VdW contacts in the calculations. Applying the same distance threshold, the total number of contacts established at the interface between the Spike glycoprotein and the $PM_{2.5}$, or its individual components (graphene, organic and inorganic molecules), have been calculated using the VMD *measure contacts* module through an in-house Tcl script. The hydrogen bonds were computed with the *Hbonds* plugin of VMD, assuming a donor-acceptor distance of 0.35 nm and bond angle of 30°. Salt bridges were calculated using the *SaltBridges* plugin of VMD, applying an oxygen-nitrogen distance cut-off of 0.32 nm.

The interaction energy between the S glycoprotein and the $PM_{2.5}$ was evaluated using the Generalized Born and Surface Area continuum solvation (MM/GBSA) method (Genheden and Ryde, 2015). MM/GBSA analysis was performed over the last 50 ns of simulation only considering S residues and glycans located at the interface with the PM carbon core, i.e. within 50 Å from the graphene layer. Non-bonded interactions (electrostatic and van der Waals (VdW) contributions) were estimated using NAMD 2.13 (Phillips et al., 2005) and final free energy of binding ($\Delta G_{binding}$) between the two molecular structures was calculated using the MolAICal program (Bai et al., 2021). Snapshots obtained from the trajectories were rendered using the VMD program.

## 3. Results

### 3.1. The SARS-CoV-2 genome RNA is detectable in the $PM_{2.5}$ quartz fiber filters

SARS-CoV-2 genomic RNA was isolated from 24 h $PM_{2.5}$ samples collected on quartz fiber filters over the period January 19th-February 6th (2021) in Bologna city area (Italy).

By performing RT-qPCR analysis, we detected the viral selected genes (*ORF-1a/b, S* and *N*) in approximately 50 % of the PM filters analyzed (Table 2), although they were never simultaneously amplified in the collected particle samples. Our data showed a positive result (amplification) for *ORF-1 a/b* gene in 6 out of 15 PM samples, with a CT ranging between 36 and 40 cycles (Fig. 1b left panel, Table 2).

Exclusively one filter (BO-PULVB-4, collected on 01/23/2021) showed the amplification (presence) of the viral *S* gene, with a CT between 38 and 40 cycles (Fig. 1b left panel, Table 2). The same filter also displayed the amplification for *ORF-1 a/b* gene (Fig. 1b left panel, Table 2).

Finally, *N* gene was only detected in 3 out of 15 filters, with a CT value ranging between 38 and 40 cycles (Fig. 1b right panel, Table 2). It was co-amplificated with *ORF-1 a/b* gene in BO-PULVB-5 and BO-PULVB-10 filters while it was singularly detected in 1 filter (BO-PULVB-1) (Table 2).

Interestingly, the filters positive for SARS-CoV-2 RNA showed a slight negative correlation with the airborne PM concentration (−0.38), suggesting again that the total mass of PM was not relevant for predicting the likelihood of finding SARS-CoV-2 markers. Noteworthy, the correlation between the number of positive SARS-CoV-2 RNA samples showed a positive strong correlation (0.59) when considering the relative enrichment of $PM_{2.5}$ in elemental carbon (f_EC), thus suggesting that, the chemical quality of the PM encountered by the virus, rather than the total mass concentration of fine PM, is the possible driver of the actual interaction and link between SARS-CoV-2 and airborne PM. Therefore, we decided to investigate by *in silico* methods the role of the PM chemical composition in the interaction with the SARS-CoV-2 virus.

### 3.2. Building the structural model of the $PM_{2.5}$

To evaluate the feasibility of a possible interaction between SARS-CoV-2 and $PM_{2.5}$ carbon core, a simplified structural model of a portion of $PM_{2.5}$ was built starting from a typical chemical composition registered in the Po Valley region during the winter season. In particular, the structural model was represented by a heterogeneous mixture of an EC core, here simplified with a graphene sheet, organic species, namely benzo[*a*]pyrene (BaP), palmitic acid (PLX), phthalic acid (PTX), levoglucosan (LVG), oxalic acid (OXC) and inorganic species, namely nitrate (NO3) and ammonium (NH4) ions (Fig. 2a). The organic and inorganic species in this model represent the secondary organic aerosol (SOA) and secondary inorganic aerosol (SIA) fractions of the $PM_{2.5}$, respectively. In Fig. 2b and c the structural model of the $PM_{2.5}$ is shown before and after the addition of the solvent, respectively. The modelled system was then subjected to a classical MD simulation which allowed organic and inorganic compounds to stratify over the graphene layer, mimicking the arrangement of aerosols around the $PM_{2.5}$ carbon core. To assess the validity of the simulation and monitor the system equilibration, RMSD of the system was calculated during the simulation run. As shown in Fig. 2d, the gradual increase of RMSD values during the first half of the simulation suggests that each component of the system is undergoing conformational sampling and equilibrating in solution. After about 120 ns of simulation, the RMSD curve reaches a plateau, indicating that the system has achieved structural and conformational stability.

**Table 2**
Analyses of the *ORF-1a/b*, *S* and *N* SARS-CoV-2 viral genes performed on $N = 15$ quartz fiber filters collected from January 19th to February 6th, (2021) in the specific area of Bologna city (Italy). The positive result (meaning the amplification of the specific genome sequence) was indicated as "X" in the table. The $PM_{2.5}$ urban background mass concentration ($PM_{2.5}$) and the relative enrichment of $PM_{2.5}$ in elemental carbon (f_EC) are also reported.

| Sample name | Date of collection (month/day/year) | ORF-1a/b | S | N | *$PM_{2.5}$ (μg:mò9-3)* [a] | *f_EC* [b] |
|---|---|---|---|---|---|---|
| BO-PULVB-1 | 01/19/2021 | | | X | 58 | 0.042 |
| BO-PULVB-2 | 01/21/2021 | | | | 84 | 0.039 |
| BO-PULVB-3 | 01/22/2021 | | | | 37 | 0.069 |
| BO-PULVB-4 | 01/23/2021 | X | X | | <3 | 0.634 |
| BO-PULVB-5 | 01/24/2021 | X | | X | 4 | 0.283 |
| BO-PULVB-6 | 01/25/2021 | | | | 12 | 0.076 |
| BO-PULVB-7 | 01/26/2021 | X | | | 9 | 0.135 |
| BO-PULVB-8 | 01/27/2021 | X | | | 14 | 0.041 |
| BO-PULVB-9 | 01/28/2021 | | | | 15 | 0.088 |
| BO-PULVB-10 | 01/29/2021 | X | | X | 31 | 0.055 |
| BO-PULVB-11 | 02/02/2021 | X | | | 27 | 0.042 |
| BO-PULVB-12 | 02/03/2021 | | | | 44 | 0.033 |
| BO-PULVB-13 | 02/04/2021 | | | | 27 | 0.051 |
| BO-PULVB-14 | 02/05/2021 | | | | 35 | 0.036 |
| BO-PULVB-15 | 02/06/2021 | | | | 19 | 0.082 |

[a] Data from https://apps.arpae.it/qualita-aria/bollettino-qa-provinciale/bo/ and selecting the data from the local urban background station "Giardini Margherita".

[b] Data kindly provided by Dr. Franco Lucarelli and colleagues of the National Institute of Nuclear Physics - Florence and collected during the RHAPS campaign held in Bologna.

#### 3.2.1. The molecular dynamics of the $PM_{2.5}$ assembly

To monitor the assembly of the $PM_{2.5}$ model and evaluate how the different organic and inorganic components stratify and interact with each other, the MD trajectory was analyzed, and Fig. 3a shows the temporal evolution of the distribution of the organic and inorganic PM species over the graphene sheet, during the 190 ns of simulation. Several organic molecules interact with the graphene layer, while other molecules interact within themselves, forming aggregates of different sizes in the solvent. Formation of these aggregates is observed already during the first steps of simulation, and mainly involves PLX, PTX and BaP molecules, as justified by the strong hydrophobic nature of these compounds (Fig. 3a and b). Once formed, these clusters tend to remain dispersed in the solvent. All the BaP molecules are trapped within the PLX clusters, while the remaining "free" PLX and PTX molecules fluctuate over the graphene and interact with the carbon sheet. LVG (Fig. 3c) and OXC (Fig. 3d) are the compounds mostly attracted to the graphene surface during the simulation. This behavior suggests that graphene can indeed act as a "adsorbing" organic molecules carbon core, in analogy to what has been observed in literature (Twigg and Phillips, 2009). On the other hand, the inorganic fraction (nitrate and ammonium ions) of the PM seem to randomly diffuse in the solvent during the simulation, without specifically approaching the graphene or establishing any stable interaction (Fig. 3e).

#### 3.2.2. Analysis of the interactions established during the $PM_{2.5}$ assembly

*3.2.2.1. Organic and inorganic molecules' diffusion on the EC core during the $PM_{2.5}$ assembly.* To characterize the degree of diffusion of the different molecules in the solvent and their distribution around the graphene sheet, mean square displacement (Fig. S1) and diffusion coefficients ($D_{coeff}$) were calculated for each compound. Fig. 4 shows the $D_{coeff}$ values for each compound as a function of simulation time. More than a half reduction in the $D_{coeff}$ of all organic molecules is observed with the increase of the simulation time, confirming that molecules tend to be constrained in their movements through the establishment of more and more interactions with the graphene or due to their insertion within hydrophobic aggregates. On the other hand, inorganic ions show no specific trend in the variations of their $D_{coeff}$, which remain higher than those of the organic counterpart during the entire simulation time (with an average of $0.8{\cdot}10^{-5}$ and $0.6{\cdot}10^{-5}$ $cm^2/s$, respectively). The casual fluctuations observed in inorganic species $D_{coeff}$ values could be explained by the occurrence of casual contact events that temporarily slow down the diffusion of these molecules. These values suggest the absence of specific hindrances to their motion, and thus that no persistent interactions with the graphene layer are established.

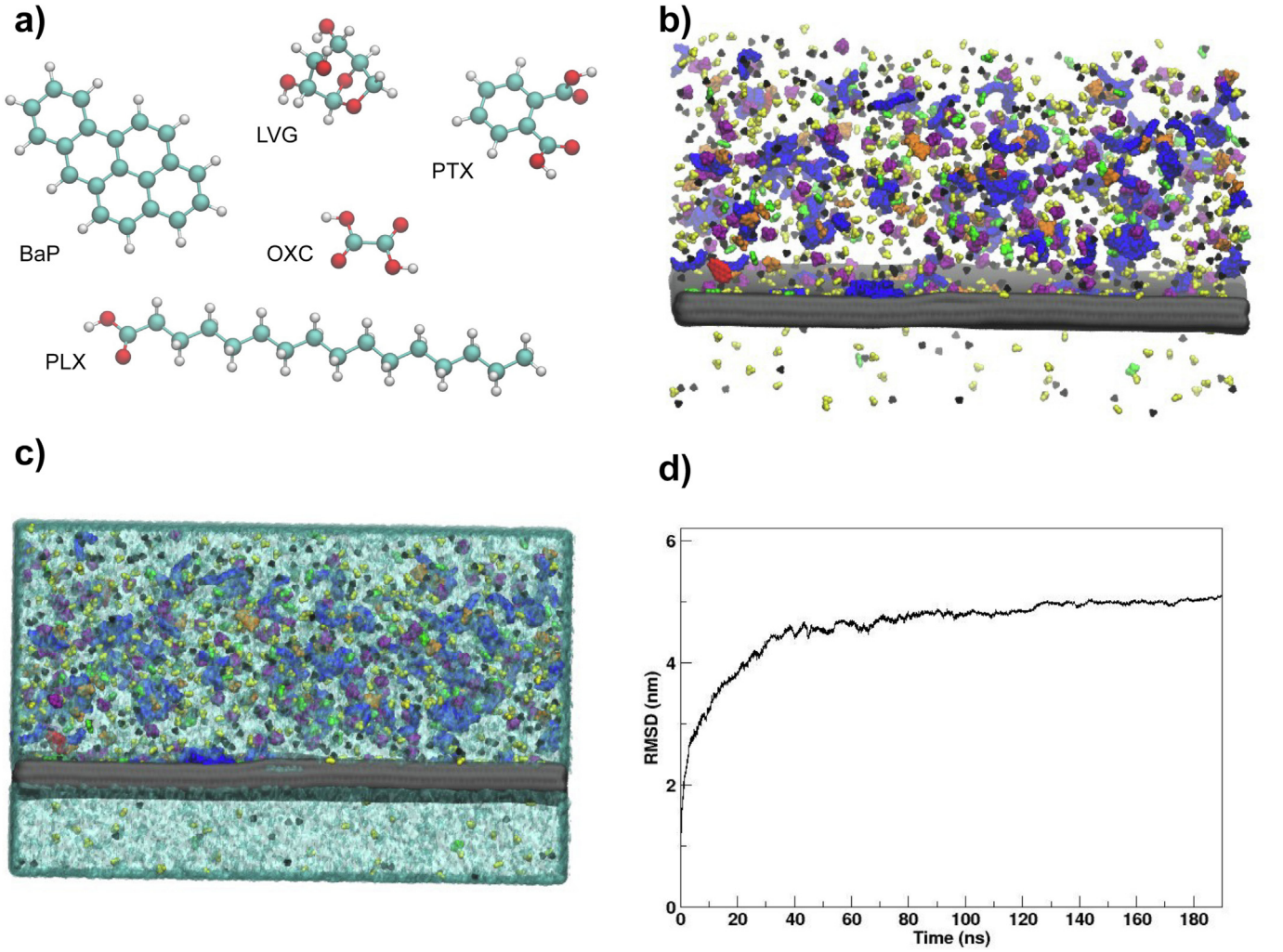


**Fig. 2.** a) Molecular structures of the benzo[*a*]pyrene (BaP), levoglucosan (LVG), phthalic acid (PTX), oxalic acid (OXC) and palmitic acid (PLX) used as representative molecules of the SOA. b) Structural model of the initial configuration of the $PM_{2.5}$ fragment before the addition of the solvent. The graphene sheet (gray) mimics the carbonaceous surface (black carbon) of the $PM_{2.5}$. Polycyclic aromatic hydrocarbons (BaP, red), carbohydrates (LVG, purple), alkaloid acids (PLX, blue), aliphatic acids (OXC, green) and aromatic acids (PTX, orange) represent the SOA component of the PM, while ammonium (NH4, black) and nitrate (NO3, yellow) represent the SIA component of the PM. c) Structural model of the initial configuration of the $PM_{2.5}$ fragment after the addition of the solvent (water molecules, cyan). d) RMSD of the atoms of the system as a function of the simulation time.

*3.2.2.2. Evaluating the adhesion of the organic molecules to the EC core of the $PM_{2.5}$.* To quantitatively evaluate the interaction of organic PM compounds with the graphene layer, for each compound, the number of contacts and the minimum distance from the graphene surface were monitored during the simulation time (Fig. 5). All molecules within 0.4 nm of graphene were considered in contact with the layer, since it is reasonable that weak interactions could be formed at this distance. After about 50 ns of simulation, the number of molecules located at $\leq 0.4$ nm from the graphene surface reaches a plateau, indicating the achievement of a stable binding and a maximum degree of surface covering (Fig. 5, right panel). Although there is no simple dependence between the molecule-graphene distances and the strength of their interactions, we consider the comparison of these minimum distances as a qualitative indicator of the stability of their contacts. In particular, the interaction of PLX and LVG with the graphene appears particularly strong since their calculated average distances are about 0.22 nm (± 0.015 nm) and 0.23 nm (± 0.022 nm), respectively (Fig. 5, left panel). These results suggest a strong anchoring of these molecules to the graphene sheet. Slightly distant interactions were recorded between the PTX (0.26 nm ± 0.022) and the OXC (0.27 nm ± 0.016) molecules with the graphene surface (Fig. 5, left panel). As expected, considering their almost complete adhesion to the graphene surface, OXC and LVG are the compounds establishing the highest number of contacts with the carbon layer (about $4{\cdot}10^3$ and $6{\cdot}10^3$ contacts, respectively) (Fig. 5, right panel). Distance analysis also highlighted that, at the beginning of the simulation, already 138 molecules are located within 0.4 nm of graphene due to the tight packing of compounds inserted in the simulation box (Table 3). After 100 ns of simulation, the number of molecules in contact within the carbon sheet is increased up to 433, while at the end of the simulation, i.e., at 190 ns, contacting molecules are 489. Therefore, at the end of the simulation, about 34 % of the selected chemical species are in direct contact with the carbon layer, the EC core of the $PM_{2.5}$. To monitor the evolution of individual compounds' attachment to graphene, the analysis was repeated considering each species separately, and averaging the calculations every 50 ns. The obtained results are consistent with the calculated $D_{coeff}$. At the end of the simulation, 97 % of the OXC molecules are bound to the carbon layer, confirming that this compound is the most attracted to the graphene hydrophobic surface. Similarly, most of the LVG (83 %) and PTX (70 %) molecules are attached to the carbon sheet at the end of the simulation. On the other hand, only 50 % of PLX molecules are located close to the graphene, while no BaP is detected within 0.4 nm of distance, confirming that these molecules, in our model, mostly form aggregates within the aqueous solvent and that, during the length of our observation (190 ns), these aggregates do not interact with the carbon layer. Notably, after an initial redistribution, the number of NO3 and NH4

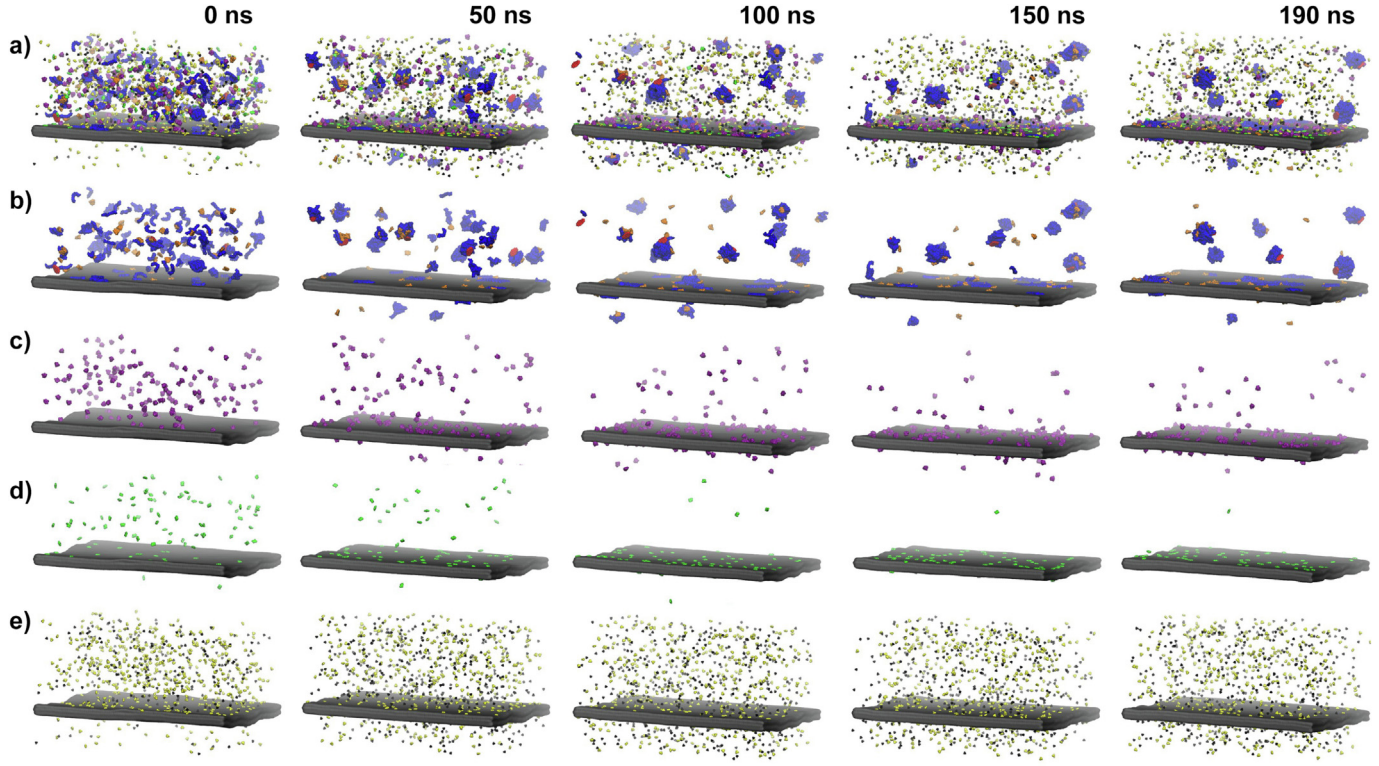


**Fig. 3.** Simulation snapshots taken at selected times of a) the whole fragment of $PM_{2.5}$, b) the BaP (red), PLX (blue), PTX (orange) molecules and the graphene sheet (gray), c) the LVG (purple) molecules and the graphene sheet (gray), d) the OXC (green) molecules and the graphene sheet (gray), d) the NO3 (yellow), NH4 (black) molecules and the graphene sheet (gray). Notes: For better visualization the water molecules are not shown.

molecules in contact with graphene remains overall stable during the simulation, confirming that these ions mostly fluctuate in the solvent and randomly distribute around the carbon sheet, without establishing any stable or specific interaction.

These findings, taken together, further indicate that most of the secondary organic compounds tend to coat or to interact with the EC core of the PM and that a proper model of $PM_{2.5}$ has been obtained at the end of the simulation.

### *3.3. Building the $PM_{2.5}$-SARS-CoV-2 interface structural model*

A simplified structural model of the $PM_{2.5}$ and SARS-CoV-2 interface was assembled **(**Fig. 6a**)** and simulated for 30 ns (data not shown).

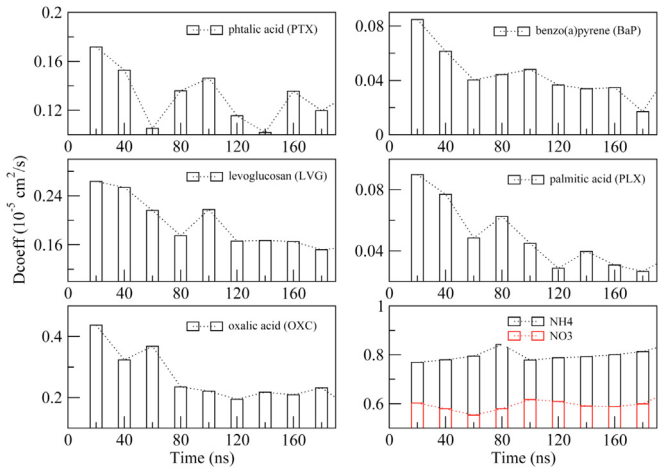


**Fig. 4.** Values of the diffusion coefficient ($D_{coeff}$), as obtained by the MSD analysis, for each compound as a function of the simulation time.

Considering the size of the final solvated system and the long computational time required for its simulation, as discussed in the Methods section, the system was reduced by including only the S "head" portion, spanning from residue 1 to 1147 **(**Fig. 6b**)**.

According to the orientation of its RBDs, the S protein can be identified in two main conformations on the virion surface: a "closed" (all RBDs down) state and an "open" (one or more RBDs up) state. Indeed, different ratios and distributions of the two distinct S conformations have been reported for intact virions (Turoňová et al., 2020; Ke et al., 2020; Yao et al., 2020), likely depending on the type of infected cells and on environmental conditions (i.e., pH, humidity). Based on this literature, at this stage we decided to simulate only the prefusion Spike glycoprotein with its three RBDs in closed configuration (Fig. 6a, and b), since in this conformation the protein is overall more stable and less prone to structural deformations when approaching and contacting a planar surface, such as the carbonaceous layer approximating the $PM_{2.5}$ core (Sahihi and Faraudo, 2022a; Sahihi and Faraudo, 2022b; Malaspina and Faraudo, 2020). This allowed us to make relevant structural comparisons with a previously performed reference simulation of the protein (Romeo et al., 2022).

#### *3.3.1. Simulation and analysis of the S glycoprotein docking to $PM_{2.5}$*

The $PM_{2.5}$–SARS-CoV-2 interface was simulated for 100 ns and, as assessed by the RMSD curve shown in Fig. 7a, the system reaches an equilibrium after 50 ns of simulation. Distance analyses show that the S protein rapidly approaches the graphene surface during the simulation, achieving a stable attachment after about 50 ns and reducing its distance from about 1.0 nm to 0.2 nm (Fig. 7b and c). This binding is maintained until the end of the simulation and is mostly due to the glycans covering the RBD and N-terminal domain (NTD), which extend towards the graphene and adhere to its surface (Fig. 7b and S2). A similar behavior has been reported by other studies characterizing Spike glycoprotein interaction with different surfaces (i.e, silver, copper, gold and polystyrene) (Sahihi and Faraudo, 2022a, 2022b).

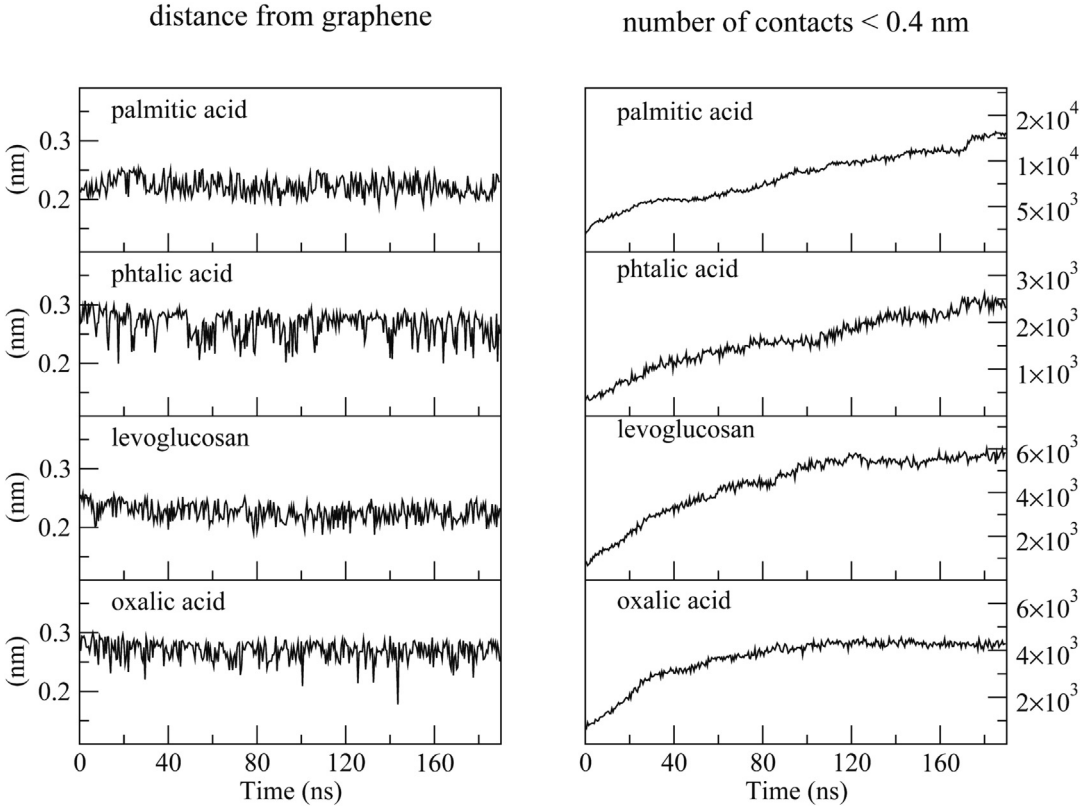


**Fig. 5.** The minimum distances (left plots) and the number of contacts at a distance <0.4 nm (right plots) between the organic molecules and the graphene surface as a function of simulation time.

Several interactions characterize the interface. Various hydrogen bonds between specific glycans and the graphene, PLX, OXC and LVG molecules (Supplementary Table S1) can be detected. In addition, some residues of the S RBD make persistent hydrogen bonds with LVG molecules, identified for >10 % over the last 50 ns of simulation (Supplementary Table S2). Contact analysis performed at the interface between the S protein and the graphene surface revealed the presence of an extensive total number of contacts, both with the complete $PM_{2.5}$ model and with individual model components (Fig. S3). In particular, up to about 4769 contacts were identified between the glycoprotein and the $PM_{2.5}$ interface (Fig. S3a). This analysis also confirmed how the glycosidic portion of the protein is the sole responsible for its attachment to the graphene surface (Fig. S3b). While the total number of contacts identified with the entire $PM_{2.5}$ model and with the individual graphene and organic components increases throughout the simulation time (Fig. S3a, S3b and S3c), the number of contacts established with the $PM_{2.5}$ inorganic portion has a constant trend, suggesting the presence of a continuous flow of the ions around the glycoprotein surface (Fig. S3d).

Finally, analysis of S glycoprotein tilt angle with respect to the z-axis normal, approximating its orientation with respect to the plane of the graphene sheets, showed that the protein stably maintains its initial orientation, perpendicular to the carbon surface, resulting in an average tilt of 10.6 ± 0.2 degrees (Fig. S4). This result further suggests a particular attraction between the upper region of the Spike and the approximated $PM_{2.5}$ carbon core, and the presence of strong interactions anchoring the protein in this binding configuration (Fig. S4).

### *3.3.2. Evaluating the binding strength between the $PM_{2.5}$ and the S glycoprotein*

The strength of the interactions established between the S protein and the $PM_{2.5}$ model has been quantified using the MM/GBSA method (Table 4). Non-bonded interactions (electrostatic and VdW contributions) have been estimated and the final free energy of binding ($\Delta G_{binding}$) between the two molecular structures has been calculated. Calculations have been performed using the last 50 ns of simulation, when the S and the $PM_{2.5}$ are already in contact and only considering S residues and glycans located at the interface with the PM carbon core, i.e., within 50 Å from the graphene layer. MM/GBSA analysis indicates that protein attachment to the carbon core (the graphene layer), together with interactions established with surrounding organic and inorganic compounds, shows an interaction energy of about −207.2 ± 3.9 kcal/mol (Table 4). The analysis highlighted the nature of this interaction which is almost completely due to dispersion forces (VdW) between the protein and the $PM_{2.5}$. The S glycoprotein shows favorable interaction energies with the organic PM compounds

**Table 3**
Average number of total and individual PM molecules in contact with the carbon layer (i.e., located within 0.4 nm of the graphene sheet), averaged for specific simulation time intervals. BaP: benzo[*a*]pyrene; LVG: levoglucosan; OXC: oxalic acid; PLX: palmitic acid; PTX: phthalic acid; NH4: ammonium; NO3: nitrate.

| Simulation interval (ns) | Average number of molecules contacting the carbon layer | | | | | | | |
|---|---|---|---|---|---|---|---|---|
| | BaP | LVG | OXC | PLX | PTX | NO3 | NH4 | Total |
| 0 | 0 | 16 (11 %) | 17 (17 %) | 13 (8 %) | 5 (10 %) | 80 (16 %) | 7 (1 %) | 138 |
| 0–50 | 0 | 82 (55 %) | 74 (74 %) | 33 (22 %) | 17 (34 %) | 147 (30 %) | 9 (2 %) | 362 |
| 50–100 | 0 | 114 (76 %) | 94 (94 %) | 51 (34 %) | 22 (44 %) | 149 (30 %) | 3 (1 %) | 433 |
| 100–150 | 0 | 116 (77 %) | 98 (98 %) | 63 (42 %) | 30 (60 %) | 148 (30 %) | 9 (2 %) | 464 |
| 150–190 | 0 | 124 (83 %) | 97 (97 %) | 75 (50 %) | 35 (70 %) | 149 (30 %) | 9 (2 %) | 489 |

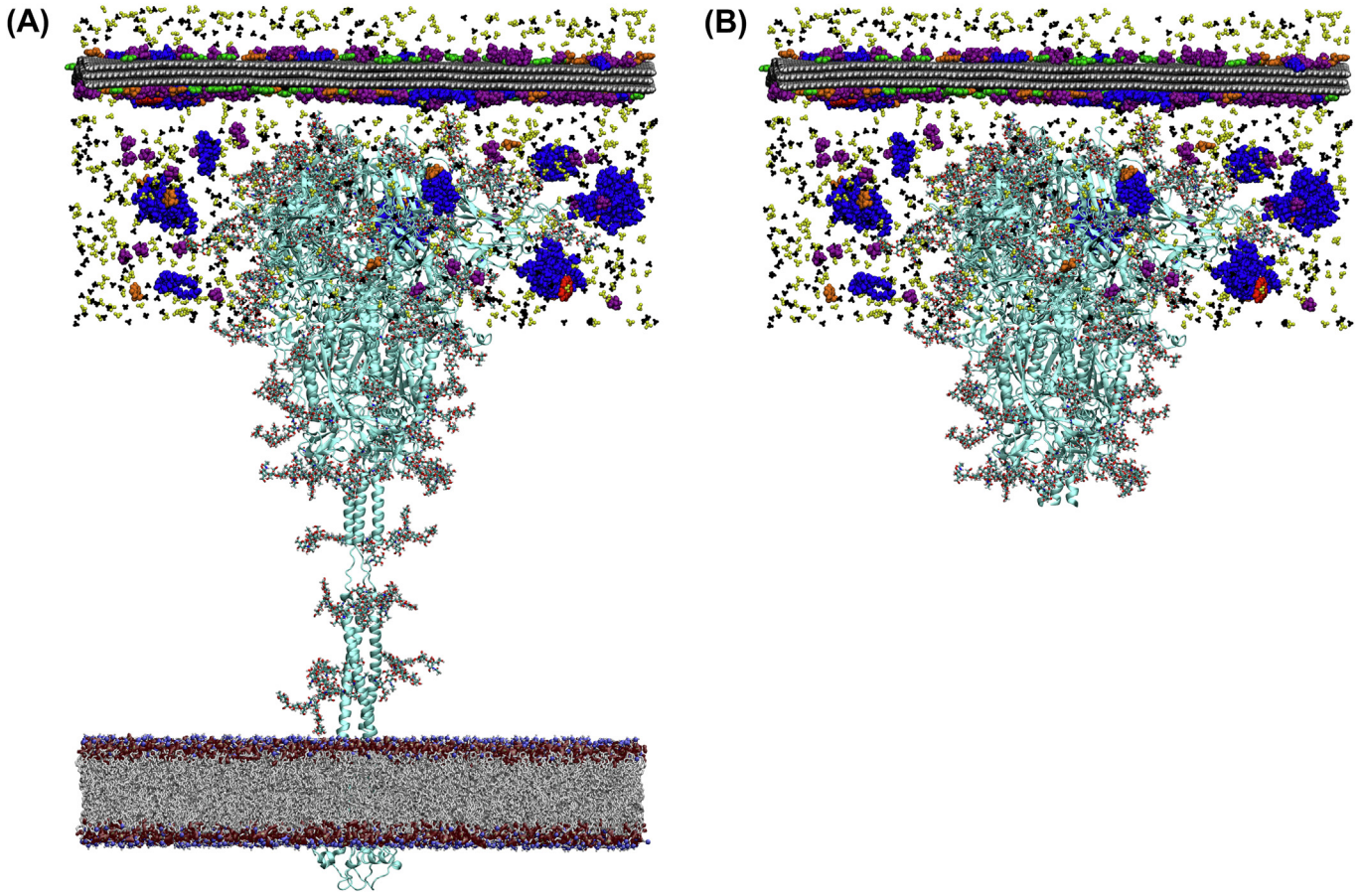


**Fig. 6.** Complete (a) and reduced (b) structural models of the Spike-PM2.5 interface. The protein is shown as ribbon in cyan, while the glycans are shown as sticks in gray. Membrane polar heads are shown as spheres, colored by atom types, while lipid tails are represented as gray sticks. The PM carbon core and its organic and inorganic components are shown as spheres, following the color coding described in Fig. 3.

and the inorganic species, evaluated as $-118.2 \pm 1.7$ kcal/mol and $-68.7 \pm 1.1$ kcal/mol, respectively (Table 4). S interactions with the organic compounds are characterized by a prominent VdW contribution, as expected due to the hydrophobic nature of most of these components. Notably, results highlighted how the S glycans are mostly involved in hydrophobic interactions with the graphene layer, showing a $\Delta G_{binding}$ of $-43.7 \pm 1.5$ kcal/mol. This value is much higher than that calculated by means of MM/GBSA for the SARS-CoV-2 S RBD and angiotensin-converting enzyme 2 (ACE2) receptor complex ($\Delta G_{bind} = -14.65 \pm 1.52$) by Forouzesh and Mishra, 2021, suggesting that the binding to PM may be stronger. S glycans also establish non-bonded contacts with the organic $PM_{2.5}$ compounds ($\Delta G_{binding} = -22.4 \pm 1.0$ kcal/mol), lower than those calculated for the protein ($\Delta G_{binding} = -83.3 \pm 1.4$ kcal/mol), and their interactions with the surrounding inorganic component are even weaker ($\Delta G_{binding} = -5.6 \pm 0.6$ kcal/mol).

Overall, the obtained values indicate that S protein interactions with the particulate model are mostly characterized by non-polar interactions. On the other hand, results suggest that the main role of the S glycans would be to contact the $PM_{2.5}$ surface through hydrophobic interactions with its carbon core, that should stabilize the virion attachment, and through non-bonded interactions with surrounding $PM_{2.5}$ organic and inorganic components.

### *3.3.3. Structural evaluation of the S glycoprotein integrity after $PM_{2.5}$ attachment*

Structural analyses have been performed on the S glycoprotein to evaluate if attachment to the $PM_{2.5}$ surface could induce an alteration in the protein's structural and functional dynamics and thus inactivate the transported virion. The obtained results have been compared to a previous trajectory of a complete model of the S inserted in a viral membrane (Romeo et al., 2022). RMSF, hydrogen bonds and salt bridges analyses have been performed only during the last 50 ns of simulation, when the protein is stably in contact with the $PM_{2.5}$ surface as clearly showed in Fig. 7c. The RMSF analysis highlighted only minor variations in the protein oscillations with respect to the reference, indicating that the protein retains its normal flexibility when attached to the $PM_{2.5}$ (Fig. 8a). Then, radius of gyration ($R_g$) of the protein has been monitored, since it approximates the distribution of protein atoms around its axis and is an indicator of the protein folding state and structural compactness. The $R_g$ calculated on the $C_\alpha$ atoms of the S protein showed limited oscillations, stably maintaining an average value of $5.05 \pm 0.01$ nm throughout the entire simulation time, same value calculated for the protein in the 150 ns reference simulation (Romeo et al., 2022) (Fig. S5). Moreover, the protein secondary structure is also stably maintained and matches that observed for the reference protein system (Fig. 8b). Total secondary structure percentages (i.e., the number of residues with each secondary structure type) are also identical for the two systems (coil: 26 %; β-sheet: 30 %; β-bridge: 1 %; bend: 13 %; turn: 9 %; α-helix: 18 %; 5-helix: 1 %; 3-helix: 2 %).

Further analysis has been focused on identifying persistent protein intra- and inter-chain hydrogen bonds and salt bridge interactions, crucial for the stability and integrity of the Spike. The patterns of interactions obtained have been compared to those observed in the reference simulation, to verify the presence of alterations induced by $PM_{2.5}$ attachment and interactions with surrounding PM compounds. For both analyses, results showed that the main interactions established are overall conserved. Concerning salt bridges, 41 persistent interactions (i.e., identified for ≥90 %

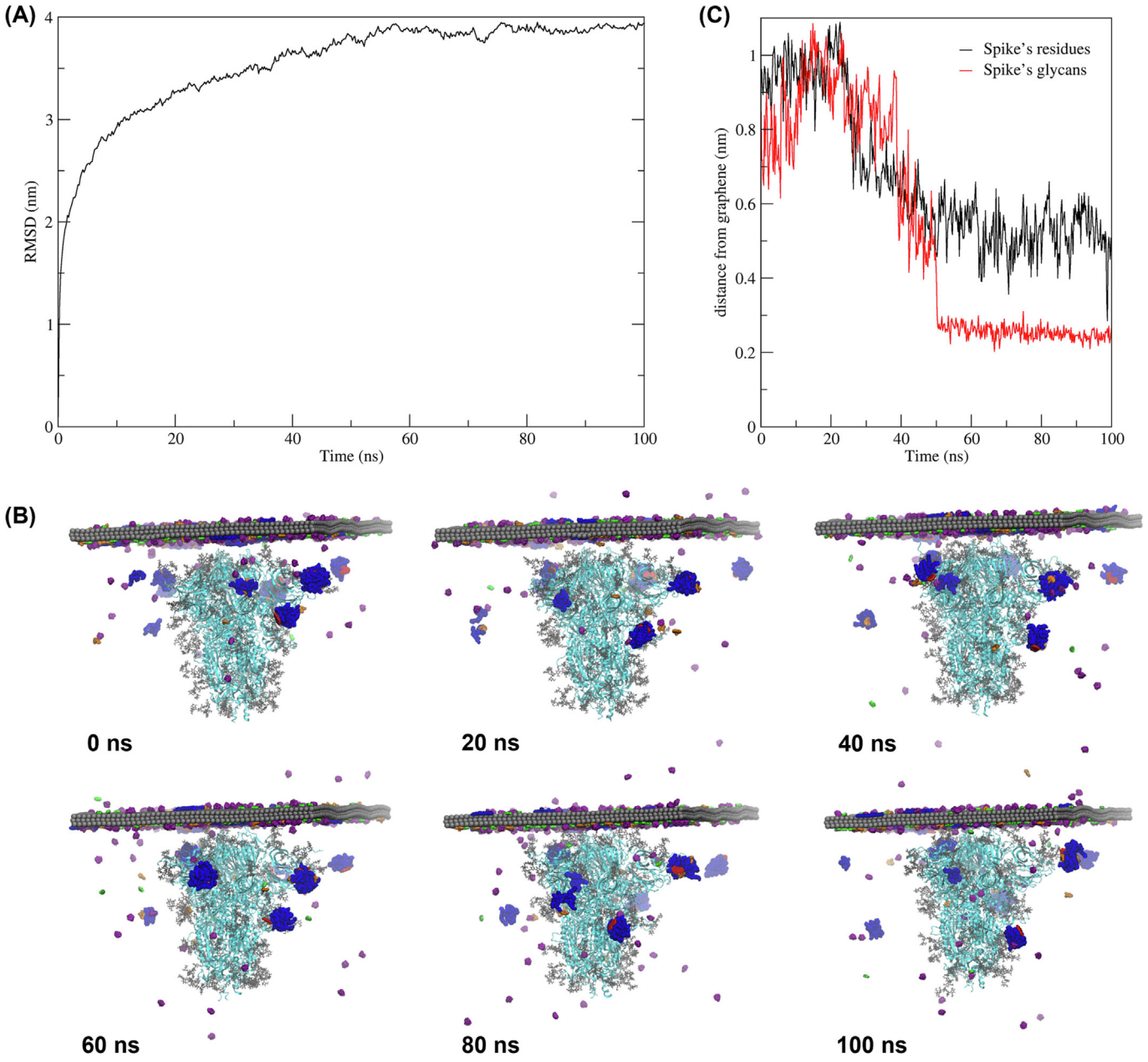


**Fig. 7.** a) RMSD of the atoms of the system as a function of simulation time. b) Simulation snapshots taken at selected times of the $PM_{2.5}$-Spike interface. The system includes the graphene sheet (gray), BaP (red), PLX (blue), PTX (orange) LVG (purple) OXC (green) molecules, the Spike protein (cyan) and the glycans (light cyan). Notes: For a better visualization the water, NH4 and NO3 molecules and K ions are not shown. c) The minimum distances from the graphene of the residues (black line) and glycans (red line) of the Spike protein as a function of simulation time.

of the simulation time) were observed in the reference simulation (Supplementary Table S3). 31 of those were also identified in the S when attached to the PM, with similar percentages ( ≥ 90.0 %). The disappearance of 7 salt bridges, and the appearance of other 8 in different locations than the reference protein was also observed. Apart from GLU465(C)-LYS462(C), neither of these salt bridges is registered in the RBD. Almost all the differences are observed in the interchain pattern indicating that the attachment to the $PM_{2.5}$ could cause a slight instability of the trimeric interactions. Concerning main hydrogen bonds interactions, even less noticeable differences were recorded between the reference structure and the protein in contact with the $PM_{2.5}$, with only three hydrogen bonds showing remarkable persistence variations between the two compared systems; the TYR496(B)-GLU406(B) hydrogen bond in the RBD region is lost when the S protein is attached to the $PM_{2.5}$ (Supplementary Table S4).

Overall, structural analyses showed that the protein maintains its structural integrity during the simulation, suggesting that the virion should retain its ability to bind the cell ACE2 receptor after being transported by $PM_{2.5}$ particles. These results also validate the choice of simulating only the larger ectodomain portion of the S glycoprotein (residues 1–1147), since its structural dynamics and flexibility are not altered in this reduced model in comparison with the complete protein structure.

## 4. Discussion

During the first phases of the pandemic, a high number of COVID-19 cases was recorded in highly polluted areas, leading to the hypothesis of a strict relationship between virus spread and infectivity and high concentration of airborne PM. From previous studies it was known that airborne PM

**Table 4**
MM/GBSA interaction energies (kcal/mol) calculated over the last 50 ns of simulation and only considering S residues and glycans located at the interface with the PM carbon core, i.e. within 50 Å from the graphene layer. Total free energies of binding($\Delta G_{binding}$) have been decomposed into van der Waal ($\Delta E_{VdW}$) and electrostatic ($\Delta E_{ele} + \Delta G_{solvent}$) contributions.

| Interactor 1 | Interactor 2 | $\Delta G_{binding}$ | $\Delta E_{ele} + \Delta G_{solvent}$ | $\Delta E_{VdW}$ |
|---|---|---|---|---|
| Protein and glycans (interface) | $PM_{2.5}$ model | −207.2 ± 3.9 | 199.8 ± 32.6 | −407.0 ± 84.8 |
| | Graphene layer | −43.8 ± 1.5 | 37.1 ± 18.0 | −81.0 ± 41.6 |
| | Organic compounds | −118.2 ± 1.7 | 69.6 ± 24.5 | −187.9 ± 44.0 |
| | Inorganic ions | −68.7 ± 1.1 | 69.4 ± 24.4 | −138.1 ± 19.4 |
| Protein (interface) | $PM_{2.5}$ model | −111.7 ± 2.1 | 92.9 ± 20.1 | −204.6 ± 36.6 |
| | Graphene layer | −5.8 ± 0.6 | −1.3 ± 9.2 | −4.4 ± 1.5 |
| | Organic compounds | −83.3 ± 1.4 | 32.1 ± 17.6 | −115.4 ± 32.1 |
| | Inorganic ions | −50.4 ± 1.0 | 34.4 ± 20.3 | −84.8 ± 17.5 |
| Glycans (interface) | $PM_{2.5}$ model | −82.6 ± 2.1 | 119.8 ± 25.4 | −202.4 ± 52.8 |
| | Graphene layer | −43.7 ± 1.5 | 32.9 ± 18.3 | −76.5 ± 40.5 |
| | Organic compounds | −22.4 ± 1.0 | 50.2 ± 18.6 | −72.5 ± 16.4 |
| | Inorganic ions | −5.6 ± 0.6 | 47.7 ± 11.4 | −53.3 ± 10.1 |

may activate and sustain pro-inflammatory responses in lung epithelial (Gualtieri et al., 2018) and endothelial cells (Pope et al., 2016) also in the presence of potential biological threats (Capasso et al., 2015). Recently, the relevance of direct and indirect effects of PM on COVID-19 severity has been analyzed (Santurtún et al., 2022), further supporting the importance of a pre-existing state of lung inflammation on the outcome of SARS-CoV-2 infection. This association has been reported also considering specific PM components, such as BaP, in patients with severe cases of COVID-19 (Rzymski et al., 2022). Therefore, PM may act as a pre-condition, facilitating the more severe forms of COVID-19 by promoting higher basal levels of pro-inflammatory mediators in the exposed population. Apart from this direct effect of pollution on host defenses and disease course, it was also hypothesized that SARS-CoV-2 could be transmitted by indirect contact via the aerosol, suggesting that PM could function as a carrier for SARS-CoV-2 virions (Nor et al., 2021).

In this study we collected samples from Bologna city area for evaluating the presence of viral particles in the PM samples. Other studies carried out in the Italian peninsula focused on the first wave of COVID-19 (Chirizzi et al., 2021; Setti et al., 2020a, 2020b, 2020c, 2020d; Pivato et al., 2021). Notably, Pivato et al. (2021) and Chirizzi et al. (2021) failed to determine SARS-CoV-2 RNA on PM samples, while Setti et al. (2020a, 2020b, 2020c, 2020d) found at least one amplified SARS-CoV-2 RNA in 20 samples out of 34. More recently, Pivato et al. (2022) reported association between PM and SARS-CoV-2 during the second COVID-19 wave. The authors reported 7 SARS-CoV-2 positive PM samples out of 38, with a ratio similar to what we were reported. These studies do not report the chemical information on the sampled PM but the mass.

Despite the positive regression between PM and COVID-19 positive cases is reported for hospital areas (Dubey et al., 2021) and for larger urban areas (Zoran et al., 2020; Madl et al., 2021), an explanatory model supporting the hypothesis that PM could function as a carrier of SARS-CoV-2 virions is still missing. The negative association between the total number of positive cases and the environmental concentration of $PM_{2.5}$ reported for the city of Milano (Zoran et al., 2020) is in contradiction with the proposed mechanism of PM as a carrier.

As recently suggested by Farhangrazi et al. (2020), the possible interaction of the virus envelope with PM may be driven, among other factors, also by specific PM chemical properties. Based on this concept we report here that, when considering the relative enrichment in EC of fine PM, the correlation between the number of SARS-CoV-2 mRNAs found in air pollution samples is high and positive (+0.59). To our knowledge, this is the first time that such a correlation is reported. Other authors (Setti et al., 2020c;

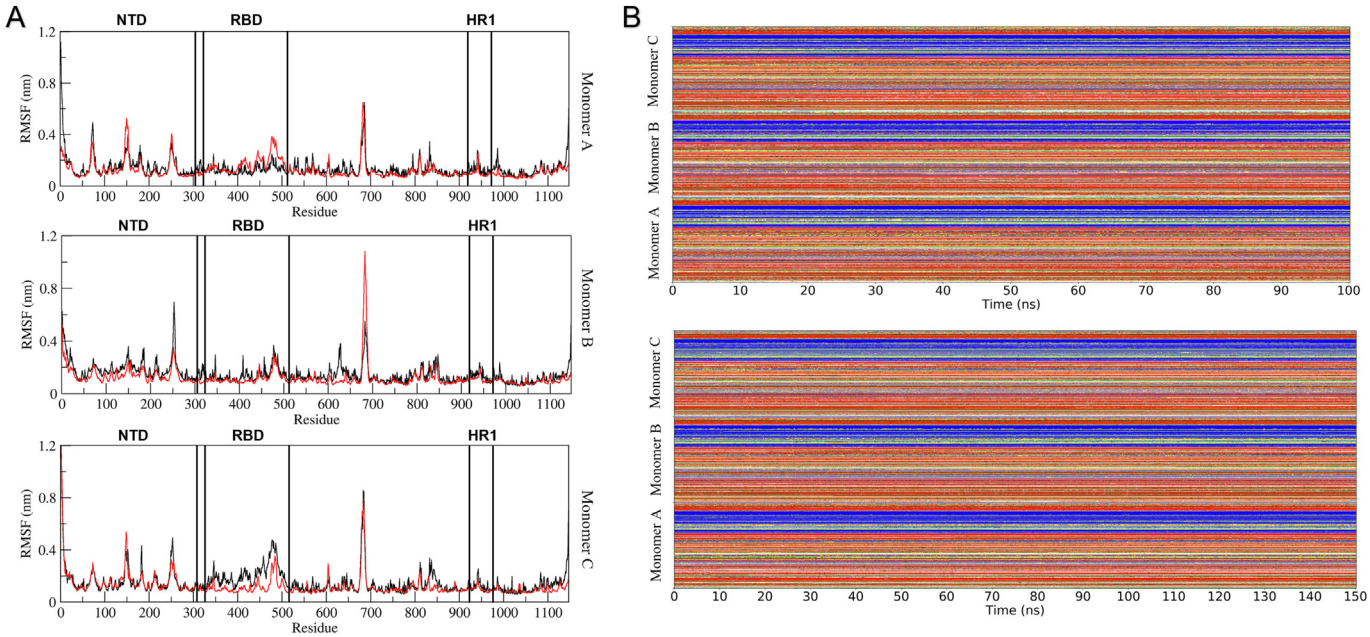


**Fig. 8.** a) RMSF analysis performed on the three Spike monomers in the $PM_{2.5}$ simulation (black lines) and in the reference simulation (Romeo et al., 2022) (red lines). Key protein domains are indicated. b) Secondary structure evolution calculated for the Spike protein in the 100 ns $PM_{2.5}$ simulation (upper image) and in the 150 ns reference simulation (lower image).

Pivato et al., 2021) detected viral mRNA markers on PM filters but they lack of any possible explanatory correlation, as we instead attempt to do in this study. Other papers reported a complete lack of association between SARS-CoV-2 virus and airborne PM (Linillos-Pradillo et al., 2021; Dunker et al., 2021). The reason for this lack of consistency may be related to several factors, such as the season of sampling, the method of sampling, the analytical procedure to extract and analyze the mRNA or the procedure to preserve filters (Licen et al., 2022; Borges et al., 2021; Pivato et al., 2021).

Despite the positive association with a specific PM component, namely the relative enrichment in EC (as we report here) or the positivity of SARS-CoV-2 mRNA detected in PM samples (as also reported by other groups), so far there is no evidence clearly demonstrating the viability of the virus associated with airborne particles. The viability time of the SARS-CoV-2 virus varies, between a few hours to some days, considering different environmental parameters (UV, relative humidity, temperature) and surface of sampling materials (Fernández-Raga et al., 2021). Moreover, a recent study (Groulx et al., 2018) showed that the binding of airborne PM may be an actual sink for viruses' infectiousness, interfering with their capability to infect a host and removing potentially infectious viral particles from the atmosphere. Therefore, the link between PM and viral particles should be carefully considered, taking into account both the possibility of PM acting as a carrier of viral particles in the lungs, or that of PM acting as a sink when viral particles are not released and remain attached to its surface.

Similarly, de La Fuente et al. (2022) showed that carbonaceous particles from diesel exhaust may act as SARS-CoV-2 virus inactivators, although coarse PM increased cellular responses. Newey et al. (2022) also reported lack of virus viability after assessing SARS-CoV-2 presence on money notes surface. Noteworthy, other than as a carrier, it has been suggested that PM may act, after interaction with SARS-CoV-2 and potentially other viruses or bacteria, as a selective pressure element forcing the emergence of new variants (Baron, 2022).

The high and positive correlation, here reported, between the number of SARS-CoV-2 mRNA and EC-enriched fine PM samples prompted us to look for any molecular interactions at a hypothetical interface represented by a carbon core with few organic and inorganic species ($PM_{2.5}$) and a fragment of SARS-CoV-2, by adopting molecular modeling and MD simulations. MD simulation is an effective method to investigate the interactions between particles on the molecular level (Hollingsworth and Dror, 2018) as well as the dynamics at several interfaces between biological molecules, including Spike and Mpro proteins of SARS-CoV-2, and several organic and inorganic surfaces (Polimeni et al., 2017; Ozboyaci et al., 2016; Malaspina and Faraudo, 2020; Sahihi and Faraudo, 2022a; Sahihi and Faraudo, 2022b; Wang et al., 2022). In this study, MD simulations were efficiently used to analyze – starting from a heterogeneous mixture of a carbon core, organic and inorganic species – the formation/assembly of a fragment of $PM_{2.5}$, and to estimate the strength of its interaction with the SARS-CoV-2 virus, here represented by the structural S protein which covers the surface of the virus.

Part of the study was devoted to building a simplified model of the $PM_{2.5}$ fragment. Indeed, the efforts reported in the literature concern the use of MD simulation for analyzing the organic aerosol formation starting from a few molecules (Karadima et al., 2019; Mansurov et al., 2018; Vardanega and Picaud, 2014) or for studying the nucleation and growth mechanisms of incipient soot particles from PAHs (Mao et al., 2017). Here, the use of MD simulation allowed, for the first time, to get some insights into different dynamic behavior and molecular interactions established by the organic (PAHs, carbohydrates, alkaloid, aromatic and aliphatic acids) and inorganic (ammonium nitrate) components with the particulate carbon core, approximated by a hydrophobic layer composed by three graphene sheets. In particular, the simulation results suggest that organic components interact more stably and specifically with the carbon core than the inorganic ions and, at the end of the simulation, about 70 % of the organic components are located close to the graphene surface. Oxalic acid, representative molecule for the aliphatic acids class, showed the highest attraction for the EC core, followed by levoglucosan, representative of the carbohydrates class, and phthalic acid, representative of the aromatic acids. Formation of clusters of aggregated palmitic acid and benzo[*a*]pyrene molecules have also been observed during the simulation, due to the intrinsic hydrophobic nature of these compounds, representing the PAHs and alkaloid acid classes, respectively.

Formation of these clusters interferes with the capability of these molecules to interact with the carbon core. Indeed, only 50 % of the palmitic acid molecules were found close to the graphene layer at the end of the simulation, while none of the five benzo[*a*]pyrene molecules were contacting this region, all being trapped within the formed palmitic acid clusters. The coordinated movements of palmitic acid and benzo[*a*]pyrene molecules are confirmed by the comparison of their diffusion coefficients, calculated at simulations intervals of 20 ns, which show a similar trend in the two molecular types. Few phthalic acids (15 out of 50) were also trapped in the palmitic acid clusters, although they show a higher tendency to interact with the graphene surface. The inorganic components of PM (nitrate and ammonium) randomly fluctuate in the solvent and they poorly interact with the carbonaceous matrix. Notably, a much higher number of $NO_3^-$ than $NH_4^+$ is observed in close contact with graphene (149 vs 9 at the end of the simulation), suggesting that the oxygen atoms may allow these ions to be more attracted to the carbon layer.

Using the final assembled $PM_{2.5}$ model, a system mimicking the binding interface between the SARS-CoV-2 Spike glycoprotein (Woo et al., 2020) and the particulate matter was generated. Following the hypothesis of a possible role of the $PM_{2.5}$ as a virus carrier, a 100 ns MD simulation of this system was performed in order to evaluate the type of interactions established at the virus-PM interface and the strength and stability of these contacts. Indeed, to act as a carrier, the PM must be able to “bind” the virus by establishing a series of more or less specific interactions with the viral surface proteins. At the same time, the stability of the bond between the PM and the virus must be maintained during all the processes of dispersion and transformation of the particulate matter in the atmosphere without compromising the molecular conformation of the viral proteins, and the integrity of the virus itself. Here, the structural integrity of the Spike glycoprotein has been monitored during the simulation through RMSF, radius of gyration, salt bridges, hydrogen bonds and secondary structure analysis, comparing the results obtained with a previous reference simulation of the protein (Romeo et al., 2022).

The results confirmed that the protein maintains its structural dynamics when adhered to the graphene layer, with no alterations observed in the protein oscillations and only minor differences detected in the pattern of intra- and inter-chain salt bridges and hydrogen bonds established. Notably, the data obtained are close to those reported for the protein structure in other computational studies investigating its interaction with different surfaces (i.e., silver, copper, gold and polystyrene), in terms of its structural stability (RMSF and $R_g$ analyses), its orientation with respect to the carbon layer, and the surface attachment mode as outlined by our simulations. Notably, the orientation parameter for the S protein in open conformation highly varies according to the type of surface considered, up to the observation of a complete distortion and adhesion of the protein structure to the surface plane (Sahihi and Faraudo, 2022a; Sahihi and Faraudo, 2022b; Malaspina and Faraudo, 2020), further supporting our choice to model the closed conformation. In fact, although in our study we only focused on the protein in its closed prefusion conformation, according to our main goal to provide a first but relevant characterization of the S protein with airborne PM, we believe that future studies should be directed towards a direct comparison of the interaction modes between the PM and the two different S protein conformations, possibly employing a complete structure of the protein inserted in a membrane mimicking the viral envelope, which would allow to obtain more accurate results and perhaps avoid the extreme tilt observed for the open conformation in the aforementioned simulation studies (Sahihi and Faraudo, 2022a; Sahihi and Faraudo, 2022b; Malaspina and Faraudo, 2020). This broader approach might also reveal other interactions between the viral S protein and the airborne PM carbonaceous surface, providing a more robust framework for a conclusive determination of the PM capability to act as a carrier for viral particles.

Another feature of the PM as a carrier is to release the virus when it encounters the host cell at the respiratory system level to allow specific binding with the ACE2 molecular target. Therefore, the strength of binding between the PM model and the virus has been estimated by using MM/GBSA, a well-established, efficient and reliable simulation method to calculate the end-point binding free energy (Genheden and Ryde, 2015). The results show that the protein glycans, which rapidly approach and attach to the carbon surface during the simulation, establish with the graphene hydrophobic interactions, showing a $\Delta G_{binding}$ of $-43.7 \pm 1.5$ kcal/mol, a value which is much higher than that obtained by Forouzesh and Mishra (2021) for the SARS-CoV-2 S RBD and ACE2 receptor complex ($\Delta G_{bind} = -14.65 \pm 1.52$). In addition, the protein attachment to the EC core (the graphene layer) and the interactions established with surrounding organic and inorganic compounds result in an interaction energy of about $-207.2 \pm 3.9$ kcal/mol. This suggests that S binding to PM may be stronger than that of the protein with the ACE2 receptor and this might lead to decreased infectivity and reduced spread by impairing the number of S proteins free to interact with target cells. Further, the possibility that the virus could be inactivated by this strong interaction with the PM cannot be excluded as observed by de la Fuente et al. (2022).

Nevertheless, the overall picture supports the hypothesis of a possible interaction between the EC core of the PM and the SARS-CoV-2 Spike proteins, suggesting that the glycans covering the upper NTDs and RBDs protein regions would be responsible for the first attachment to the $PM_{2.5}$ carbon core, while the protein itself and the remaining glycans would be trapped by the surrounding cloud of organic and inorganic $PM_{2.5}$ components through a network of non-bonded interactions, which could stabilize the virion for airborne transport. However, despite the interaction energies obtained seem to suggest the presence of a strong affinity between the Spike and the $PM_{2.5}$, it should be emphasized that these values do not assess whether the established interactions would be sufficient to stably carry the virus in the atmosphere, or whether the virus would retain its activity after the transport.

## 5. Conclusion

In this study, we aimed to investigate the possibility that $PM_{2.5}$ may act as a carrier of SARS-CoV-2 through an innovative approach that integrates molecular and *in silico* methods. The approach, starting from the identification of the SARS-CoV-2 genome on $PM_{2.5}$ quartz filters collected in the area of Bologna during winter 2021, exploits a *in silico* analysis of the molecular interactions between the virus surface and a model of fine PM. We found a positive correlation between PM elemental carbon content and SARS-CoV-2 mRNA markers. The nature and the strength of the putative molecular interactions occurring between the $PM_{2.5}$ carbon core surface and the Spike glycoprotein, representing the first contact region of the virus, have been estimated through different computational analyses. In particular, the MD simulations highlighted that the glycans of the Spike protein play a crucial role during the attachment process to the PM elemental carbon core and analyses of the Spike protein structural features revealed that its adhesion to the PM did not cause any significant tertiary or secondary structural changes in the protein conformation. We found that the adhesion energy, estimated through MM/GBSA method, is stronger than that reported for the Spike protein and the ACE2 receptor binding.

Therefore, the association between the PM and SARS-CoV-2 appears plausible. However, whether this mechanism would then result in an actual transport and release of the virus to the human ACE2 receptor once the particles have been inhaled, or whether the virus would retain its activity after the transport, are key aspects that still need to be verified by further experimental analysis. Although our study has some limitations, since further and more accurate efforts are still necessary to confirm the actual interaction between SARS-CoV-2 and the PM, nonetheless, the approach provides a first step in the understanding the molecular interplay between the chemical nature of the PM and the virus. The relevance of the reported findings resides in providing for the first time a positive association with a specific PM component, namely the EC, and a first insight into the fundamental physicochemical aspects of the virus-PM interaction, crucial to identify the factors making the virus(es) prone to PM adhesion. In view of our findings, previous association between PM mass concentration and SARS-CoV-2 presence, reported in the literature, should be revised in term of relative enrichment in EC. This revision could provide more meaningful data to interpret the ecological and epidemiological associations between PM and COVID-19 incidence. The strength of our applied *in silico* approach lies in the ability, in principle, of modeling different types of PM by varying both the concentration and the chemical composition of the airborne pollutants. The use of molecular modeling and MD simulations to model different PM compositions may represent not only a great opportunity for understanding the PM formation processes but also, in analogy to the well-established drug delivery techniques widely used in the biomedical field, a useful tool to rapidly evaluate the possible interaction of PM with viruses, bacteria or other relevant cellular targets. This possibility may ultimately result in an additional asset to counteract or control the spread of future airborne diseases in highly polluted regions and could provide new and relevant information that could be helpful for air pollution control plans.

## CRediT authorship contribution statement

**Alice Romeo:** Methodology, Formal analysis, Visualization, Investigation, Writing - original draft, Writing - review & editing. **Roberto Pellegrini:** Methodology, Formal analysis, Investigation. **Maurizio Gualtieri:** Conceptualization, Investigation, Data curation, Writing – original draft, Writing – review & editing. **Barbara Benassi:** Conceptualization, Methodology, Investigation, Data curation, Writing – original draft, Writing – review & editing, Supervision. **Massimo Santoro:** Methodology, Investigation, Writing – original draft, Writing – review & editing. **Federico Iacovelli:** Methodology, Investigation. **Milena Stracquadanio:** Investigation. **Mattia Falconi:** Investigation, Writing – original draft, Writing – review & editing, Supervision. **Carmela Marino:** Conceptualization, Funding acquisition. **Gabriele Zanini:** Conceptualization, Project administration, Funding acquisition. **Caterina Arcangeli:** Conceptualization, Methodology, Formal analysis, Data curation, Writing – original draft, Writing – review & editing, Visualization, Supervision.

## Data availability

Data will be made available on request.

## Declaration of competing interest

The authors declare that they have no known competing financial interests or personal relationships that could have appeared to influence the work reported in this paper.

## Acknowledgements

We acknowledge the PULVIRUS Project (www.pulvirus.it) that funded this activity and the colleagues from the National and Regional Environmental Agencies involved in the Project. The computing resources used for this work were provided by the CRESCO/ENEAGRID High Performance Computing infrastructure and its staff (Iannone et al., 2019). The infrastructure is funded by ENEA, the Italian National Agency for New Technologies, Energy and Sustainable Economic Development and by Italian and European research programs (http://www.cresco.enea.it/english). The authors thank the ENEA colleagues: Dr. Guido Guarnieri for his technical support to the access to computational resources, Dr. Paola Giardullo for her support in the analysis of the quartz filter, Dr. Ilaria D'Elia and Dr. Antonio Piersanti for their comments. The authors thank Dr. Franco Lucarelli, Dr. Giulia Calzolai and Dr. Silvia Nava of the National Institute for Nuclear Physics (INFN) in Florence for sharing the EC data collected during the PM characterization campaign performed for the RHAPS project.

Icons for the graphical abstract were made by ultimatearm, Eucalyp and Freepik from www.flaticon.com.

## Appendix A. Supplementary data

Supplementary data to this article can be found online at https://doi.org/10.1016/j.scitotenv.2023.165059.

## References


Abraham, M.J., Murtola, T., Schulz, R., Páll, S., Smith, J.C., Hess, B., Lindahl, E., 2015. Gromacs: high performance molecular simulations through multi-level parallelism from laptops to supercomputers. SoftwareX 1-2, 19–25. https://doi.org/10.1016/j.softx.2015.06.001.

Al Huraimel, K., Alhosani, M., Kunhabdulla, S., Stietiya, M.H., 2020. SARS-CoV-2 in the environment: modes of transmission, early detection and potential role of pollutions. Sci. Total Environ. 744, 140946. https://doi.org/10.1016/j.scitotenv.2020.140946.

Anand, U., Cabreros, C., Mal, J., Ballesteros, F., Sillanpää, M., Tripathi, V., Bontempi, E., 2021. Novel coronavirus disease 2019 (COVID-19) pandemic: from transmission to control with an interdisciplinary vision. Environ. Res. 197, 111126. https://doi.org/10.1016/j.envres.2021.111126.

Bai, Q., Tan, S., Xu, T., Liu, H., Huang, J., Yao, X., 2021. MolAICal: a soft tool for 3D drug design of protein targets by artificial intelligence and classical algorithm. Brief. Bioinform. 22, bbaa161. https://doi.org/10.1093/bib/bbaa161.

Barakat, T., Muylkens, B., Su, B.-L., 2020. Is particulate matter of air pollution a vector of Covid-19 pandemic? Matter 3, 977–980. https://doi.org/10.1016/j.matt.2020.09.014.

Baron, Y.M., 2022. Are there medium to short-term multifaceted effects of the airborne pollutant PM2.5 determining the emergence of SARS-CoV-2 variants? Med. Hypotheses 158, 110718. https://doi.org/10.1016/j.mehy.2021.110718.

Belosi, F., Conte, M., Gianelle, V., Santachiara, G., Contini, D., 2021. On the concentration of SARS-CoV-2 in outdoor air and the interaction with pre-existing atmospheric particles. Environ. Res. 193, 110603. https://doi.org/10.1016/j.envres.2020.110603.

Bontempi, E., 2020. First data analysis about possible COVID-19 virus airborne diffusion due to air particulate matter (PM): the case of Lombardy (Italy). Environ. Res. 186, 109639. https://doi.org/10.1016/j.envres.2020.109639.

Borges, J.T., Nakada, L.Y.K., Maniero, M.G., Guimarães, J.R., 2021. SARS-CoV-2: a systematic review of indoor air sampling for virus detection. Environ. Sci. Pollut. Res. 28, 40460–40473. https://doi.org/10.1007/s11356-021-13001-w.

Capasso, L., Longhin, E., Caloni, F., Camatini, M., Gualtieri, M., 2015. Synergistic inflammatory effect of PM10 with mycotoxin deoxynivalenol on human lung epithelial cells. Toxicon 104, 65–72. https://doi.org/10.1016/j.toxicon.2015.08.008.

Chirizzi, D., Conte, M., Feltracco, M., Dinoi, A., Gregoris, E., Barbaro, E., La Bella, G., Ciccarese, G., La Salandra, G., Gambaro, A., Contini, D., 2021. SARS-CoV-2 concentrations and virus-laden aerosol size distributions in outdoor air in north and south of Italy. Environ. Int. 146, 106255. https://doi.org/10.1016/j.envint.2020.106255.

Chung, K.F., Abubakar-Waziri, H., Kalaiarasan, G., Adcock, I.M., Dilliway, C., Fang, F., Pain, C., Kumar, P., Ransome, E., Savolainen, V., Bhavsar, P., Porter, A., 2022. SARS-CoV2 and air pollution interactions: airborne transmission and COVID-19. Mol. Front. J. 1–6. https://doi.org/10.1142/S2529732522400016.

Coccia, M., 2020. Factors determining the diffusion of COVID-19 and suggested strategy to prevent future accelerated viral infectivity similar to COVID. Sci. Total Environ. 729, 138474. https://doi.org/10.1016/j.scitotenv.2020.138474.

Comunian, S., Dongo, D., Milani, C., Palestini, P., 2020. Air pollution and Covid-19: the role of particulate matter in the spread and increase of Covid-19's morbidity and mortality. Int. J. Environ. Res. Public Health 17. https://doi.org/10.3390/ijerph17124487.

Costabile, F., Decesari, S., Vecchi, R., Lucarelli, F., Curci, G., Massabò, D., Rinaldi, M., Gualtieri, M., Corsini, E., Menegola, E., Canepari, S., Massimi, L., Argentini, S., Busetto, M., Di Iulio, G., Di Liberto, L., Paglione, M., Petenko, I., Russo, M., Marinoni, A., Casasanta, G., Valentini, S., Bernardoni, V., Crova, F., Valli, G., Forello, A.C., Giardi, F., Nava, S., Pazzi, G., Prati, P., Vernocchi, V., La Torretta, T., Petralia, E., Stracquadanio, M., Zanini, G., Melzi, G., Nozza, E., Iulini, M., Caruso, D., Cioffi, L., Imperato, G., Giavarini, F., Battistoni, M., Di Renzo, F., Frezzini, M.A., Perrino, C., Facchini, M.C., 2022. On the redox-activity and health-effects of atmospheric primary and secondary aerosol: phenomenology. Atmosphere 13, 704. https://doi.org/10.3390/atmos13050704.

Darden, T., York, D., Pedersen, L., 1993. Particle mesh Ewald: an N·log(N) method for Ewald sums in large systems. J. Chem. Phys. 98, 10089. https://doi.org/10.1063/1.464397.

de la Fuente, J., Armas, O., Barroso-Arévalo, S., Gortázar, C., García-Seco, T., Buendía-Andrés, A., Villanueva, F., Soriano, J.A., Mazuecos, L., Vaz-Rodrigues, R., García-Contreras, R., García, A., Monsalve-Serrano, J., Domínguez, L., Sánchez-Vizcaíno, J.M., 2022. Good and bad get together: inactivation of SARS-CoV-2 in particulate matter pollution from different fuels. Sci. Total Environ. 844, 157241. https://doi.org/10.1016/j.scitotenv.2022.157241.

Domingo, J.L., Rovira, J., 2020. Effects of air pollutants on the transmission and severity of respiratory viral infections. Environ. Res. 187, 109650. https://doi.org/10.1016/j.envres.2020.109650.

Dubey, A., Kotnala, G., Mandal, T.K., Sonkar, S.C., Singh, V.K., Guru, S.A., Bansal, A., Irungbam, M., Husain, F., Goswami, B., Kotnala, R.K., Saxena, S., Sharma, S.K., Saxena, K.N., Sharma, C., Kumar, S., Aswal, D.K., Manchanda, V., Koner, B.C., 2021. Evidence of the presence of SARS-CoV-2 virus in atmospheric air and surfaces of a dedicated COVID hospital. J. Med. Virol. 93, 5339–5349. https://doi.org/10.1002/jmv.27029.

Dunker, S., Hornick, T., Szczepankiewicz, G., Maier, M., Bastl, M., Bumberger, J., Treudler, R., Liebert, U.G., Simon, J.-C., 2021. No SARS-CoV-2 detected in air samples (pollen and particulate matter) in Leipzig during the first spread. Sci. Total Environ. 755, 142881. https://doi.org/10.1016/j.scitotenv.2020.142881.

EEA, 2022. Air quality in Europe 2022. European Environment Agency https://doi.org/10.2800/488115. https://www.eea.europa.eu/publications/air-quality-in-europe-2022.

Farhangrazi, Z.S., Sancini, G., Hunter, A.C., Moghimi, S.M., 2020. Airborne particulate matter and SARS-CoV-2 partnership: virus hitchhiking, stabilization and immune cell targeting — a hypothesis. Front. Immunol. 11, 579352. https://doi.org/10.3389/fimmu.2020.579352.

Feller, S.E., Zhang, Y., Pastor, R.W., Brooks, B.R., 1995. Constant pressure molecular dynamics simulation: the Langevin piston method. J. Chem. Phys. 103, 4613–4621. https://doi.org/10.1063/1.470648.

Fernández-Raga, M., Díaz-Marugán, L., García Escolano, M., Bort, C., Fanjul, V., 2021. SARS-CoV-2 viability under different meteorological conditions, surfaces, fluids and transmission between animals. Environ. Res. 192, 110293. https://doi.org/10.1016/j.envres.2020.110293.

Forouzesh, N., Mishra, N., 2021. An effective MM/GBSA protocol for absolute binding free energy calculations: a case study on SARS-CoV-2 spike protein and the human ACE2 receptor. Molecules 26, 2383. https://doi.org/10.3390/molecules26082383.

Genheden, S., Ryde, U., 2015. The MM/PBSA and MM/GBSA methods to estimate ligand-binding affinities. Expert Opin. Drug Discovery 10, 449–461. https://doi.org/10.1517/17460441.2015.1032936.

Goga, N., Rzepiela, A.J., de Vries, A.H., Marrink, S.J., Berendsen, H.J., 2012. Efficient algorithms for Langevin and DPD dynamics. J. Chem. Theory Comput. 8, 3637–3649. https://doi.org/10.1021/ct3000876.

Groulx, N., Urch, B., Duchaine, C., Mubareka, S., Scott, J.A., 2018. The pollution particulate concentrator (PoPCon): a platform to investigate the effects of particulate air pollutants on viral infectivity. Sci. Total Environ. 628–629, 1101–1107. https://doi.org/10.1016/j.scitotenv.2018.02.118.

Gualtieri, M., Grollino, M.G., Consales, C., Costabile, F., Manigrasso, M., Avino, P., Aufderheide, M., Cordelli, E., Di Liberto, L., Petralia, E., Raschellà, G., Stracquadanio, M., Wiedensohler, A., Pacchierotti, F., Zanini, G., 2018. Is it the time to study air pollution effects under environmental conditions? A case study to support the shift of in vitro toxicology from the bench to the field. Chemosphere 207, 552–564. https://doi.org/10.1016/j.chemosphere.2018.05.130.

Hollingsworth, S.A., Dror, R.O., 2018. Molecular dynamics simulation for all. Neuron 99, 1129–1143. https://doi.org/10.1016/j.neuron.2018.08.011.

Humphrey, W., Dalke, A., Schulten, K., 1996. VMD: visual molecular dynamics. J. Mol. Graph. 14 (33–38), 27–28. https://doi.org/10.1016/0263-7855(96)00018-5.

Iannone, F., Ambrosino, F., Bracco, G., De Rosa, M., Funel, A., Guarnieri, G., Migliori, S., Palombi, F., Ponti, G., Santomauro, G., Procacci, P., 2019. CRESCO ENEA HPC clusters: A working example of a multifabric GPFS Spectrum scale layout. 2019 International Conference on High Performance Computing & Simulation (HPCS). Presented at the 2019 International Conference on High Performance Computing & Simulation (HPCS), pp. 1051–1052 https://doi.org/10.1109/HPCS48598.2019.9188135.

Jo, S., Kim, T., Iyer, V.G., Im, W., 2008. CHARMM-GUI: a web-based graphical user interface for CHARMM. J. Comput. Chem. 29, 1859–1865. https://doi.org/10.1002/jcc.20945.

Jorgensen, W.L., Chandrasekhar, J., Madura, J.D., Impey, R.W., Klein, M.L., 1983. Comparison of simple potential functions for simulating liquid water. J. Chem. Phys. 79, 926–935. https://doi.org/10.1063/1.445869.

Karadima, K.S., Mavrantzas, V.G., Pandis, S.N., 2019. Insights into the morphology of multicomponent organic and inorganic aerosols from molecular dynamics simulations. Atmos. Chem. Phys. 19, 5571–5587. https://doi.org/10.5194/acp-19-5571-2019.

Kayalar, Ö., Arı, A., Babuçcu, G., Konyalılar, N., Doğan, Ö., Can, F., Şahin, Ü.A., Gaga, E.O., Levent Kuzu, S., Arı, P.E., Odabaşı, M., Taşdemir, Y., Sıddık Cindoruk, S., Esen, F., Sakın, E., Çalışkan, B., Tecer, L.H., Fıçıcı, M., Altın, A., Onat, B., Ayvaz, C., Uzun, B., Saral, A., Döğeroğlu, T., Malkoç, S., Üzmez, Ö.Ö., Kunt, F., Aydın, S., Kara, M., Yaman, B., Doğan, G., Olgun, B., Dokumacı, E.N., Güllü, G., Uzunpınar, E.S., Bayram, H., 2021. Existence of SARS-CoV-2 RNA on ambient particulate matter samples: a nationwide study in Turkey. Sci. Total Environ. 789, 147976. https://doi.org/10.1016/j.scitotenv.2021.147976.

Ke, Z., Oton, J., Qu, K., Cortese, M., Zila, V., McKeane, L., Nakane, T., Zivanov, J., Neufeldt, C.J., Cerikan, B., Lu, J.M., Peukes, J., Xiong, X., Kräusslich, H.G., Scheres, S.H.W., Bartenschlager, R., Briggs, J.A.G., 2020. Structures and distributions of SARS-CoV-2 spike proteins on intact virions. Nature. 588, 498–502. https://doi.org/10.1038/s41586-020-2665-2.

Kim, S., Chen, J., Cheng, T., Gindulyte, A., He, J., He, S., Li, Q., Shoemaker, B.A., Thiessen, P.A., Yu, B., Zaslavsky, L., Zhang, J., Bolton, E.E., 2021. PubChem in 2021: new data content and improved web interfaces. Nucleic Acids Res. 49, D1388–D1395. https://doi.org/10.1093/nar/gkaa971.

Kumar, S., Singh, R., Kumari, N., Karmakar, S., Behera, M., Siddiqui, A.J., Rajput, V.D., Minkina, T., Bauddh, K., Kumar, N., 2021. Current understanding of the influence of environmental factors on SARS-CoV-2 transmission, persistence, and infectivity. Environ. Sci. Pollut. Res. Int. 28, 6267–6288. https://doi.org/10.1007/s11356-020-12165-1.

Licen, S., Zupin, L., Martello, L., Torboli, V., Semeraro, S., Gardossi, A.L., Greco, E., Fontana, F., Crovella, S., Ruscio, M., Palmisani, J., Di Gilio, A., Piscitelli, P., Pallavicini, A., Barbieri, P., 2022. SARS-CoV-2 RNA recovery from air sampled on quartz Fiber filters: a matter of sample preservation? Atmosphere 13, 340. https://doi.org/10.3390/atmos13020340.

Linillos-Pradillo, B., Rancan, L., Ramiro, E.D., Vara, E., Artíñano, B., Arias, J., 2021. Determination of SARS-CoV-2 RNA in different particulate matter size fractions of outdoor air samples in Madrid during the lockdown. Environ. Res. 195, 110863. https://doi.org/10.1016/j.envres.2021.110863.

Madl, P., Arvay, C., Gatti, A., Giuliani, L., Lettner, H., 2021. Air pollution, SARS-CoV-2 and the wider implications - an overview of recent events with a focus on Italy. Aerosol Air Qual. Res. 21, 200438. https://doi.org/10.4209/aaqr.200438.

Malaspina, D.C., Faraudo, J., 2020. Computer simulations of the interaction between SARS-CoV-2 spike glycoprotein and different surfaces. Biointerphases 15, 051008. https://doi.org/10.1116/6.0000502.

Maleki, M., Anvari, E., Hopke, P.K., Noorimotlagh, Z., Mirzaee, S.A., 2021. An updated systematic review on the association between atmospheric particulate matter pollution and prevalence of SARS-CoV-2. Environ. Res. 195, 110898. https://doi.org/10.1016/j.envres.2021.110898.

Mansurov, U., Shah, D., Bazybek, N., Amouei Torkmahalleh, M., 2018. Particulate matter formation in post-combustion CO2 capture columns: insights from molecular dynamics simulations. Energy Fuel 32, 12679–12688. https://doi.org/10.1021/acs.energyfuels.8b02647.

Mao, Q., van Duin, A.C.T., Luo, K.H., 2017. Formation of incipient soot particles from polycyclic aromatic hydrocarbons: a ReaxFF molecular dynamics study. Carbon 121, 380–388. https://doi.org/10.1016/j.carbon.2017.06.009.

Martelletti, L., Martelletti, P., 2020. Air pollution and the novel Covid-19 disease: a putative disease risk factor. SN Compr. Clin. Med. 2, 383–387. https://doi.org/10.1007/s42399-020-00274-4.

Martínez, L., Andrade, R., Birgin, E.G., Martínez, J.M., 2009. PACKMOL: a package for building initial configurations for molecular dynamics simulations. J. Comput. Chem. 30, 2157–2164. https://doi.org/10.1002/jcc.21224.

Martyna, G.J., Tobias, D.J., Klein, M.L., 1994. Constant pressure molecular dynamics algorithms. J. Chem. Phys. 101, 4177–4189. https://doi.org/10.1063/1.467468.

Newey, C.R., Olausson, A.T., Applegate, A., Reid, A.-A., Robison, R.A., Grose, J.H., 2022. Presence and stability of SARS-CoV-2 on environmental currency and money cards in Utah reveals a lack of live virus. PLoS One 17, e0263025. https://doi.org/10.1371/journal.pone.0263025.

Nor, N.S.M., Yip, C.W., Ibrahim, N., Jaafar, M.H., Rashid, Z.Z., Mustafa, N., Hamid, H.H.A., Chandru, K., Latif, M.T., Saw, P.E., Lin, C.Y., Alhasa, K.M., Hashim, J.H., Nadzir, M.S.M., 2021. Particulate matter (PM2.5) as a potential SARS-CoV-2 carrier. Sci. Rep. 11, 2508. https://doi.org/10.1038/s41598-021-81935-9.

Ozboyaci, M., Kokh, D.B., Corni, S., Wade, R.C., 2016. Modeling and simulation of protein–surface interactions: achievements and challenges. Q. Rev. Biophys. 49, e4. https://doi.org/10.1017/S0033583515000256.

Phillips, J.C., Braun, R., Wang, W., Gumbart, J., Tajkhorshid, E., Villa, E., Chipot, C., Skeel, R.D., Kalé, L., Schulten, K., 2005. Scalable molecular dynamics with NAMD. J. Comput. Chem. 26, 1781–1802. https://doi.org/10.1002/jcc.20289.

Pietrogrande, M.C., Bacco, D., Rossi, M., 2013. Chemical characterization of polar organic markers in aerosols in a local area around Bologna, Italy. Atmos. Environ. 75, 279–286. https://doi.org/10.1016/j.atmosenv.2013.04.023.

Pivato, A., Amoruso, I., Formenton, G., Di Maria, F., Bonato, T., Vanin, S., Marion, A., Baldovin, T., 2021. Evaluating the presence of SARS-CoV-2 RNA in the particulate matters during the peak of COVID-19 in Padua, northern Italy. Sci. Total Environ. 784, 147129. https://doi.org/10.1016/j.scitotenv.2021.147129.

Pivato, A., Formenton, G., Di Maria, F., Baldovin, T., Amoruso, I., Bonato, T., Mancini, P., Bonanno Ferraro, G., Veneri, C., Iaconelli, M., Bonadonna, L., Vicenza, T., La Rosa, G., Suffredini, E., 2022. SARS-CoV-2 in atmospheric particulate matter: an experimental survey in the province of Venice in northern Italy. Int. J. Environ. Res. Public Health 19, 9462. https://doi.org/10.3390/ijerph19159462.

Polimeni, M., Petridis, L., Smith, J.C., Arcangeli, C., 2017. Dynamics at a peptide-TiO2 Anatase (101) Interface. J. Phys. Chem. B 121, 8869–8877. https://doi.org/10.1021/acs.jpcb.7b04707.

Pope, C.A., Bhatnagar, A., McCracken, J.P., Abplanalp, W., Conklin, D.J., O'Toole, T., 2016. Exposure to fine particulate air pollution is associated with endothelial injury and systemic inflammation. Circ. Res. 119, 1204–1214. https://doi.org/10.1161/CIRCRESAHA.116.309279.

Richards, L.A., Schäfer, A.I., Richards, B.S., Corry, B., 2012. The importance of dehydration in determining ion transport in narrow pores. Small 8, 1701–1709. https://doi.org/10.1002/smll.201102056.

Romeo, A., Iacovelli, F., Scagnolari, C., Scordio, M., Frasca, F., Condò, R., Ammendola, S., Gaziano, R., Anselmi, M., Divizia, M., Falconi, M., 2022. Potential use of tea tree oil as a disinfectant agent against coronaviruses: a combined experimental and simulation study. Molecules 27, 3786. https://doi.org/10.3390/molecules27123786.

Rzymski, P., Poniedziałek, B., Rosińska, J., Rogalska, M., Zarębska-Michaluk, D., Rorat, M., Moniuszko-Malinowska, A., Lorenc, B., Kozielewicz, D., Piekarska, A., Sikorska, K., Dworzańska, A., Bolewska, B., Angielski, G., Kowalska, J., Podlasin, R., Oczko-Grzesik, B., Mazur, W., Szymczak, A., Flisiak, R., 2022. The association of airborne particulate matter and benzo[a]pyrene with the clinical course of COVID-19 in patients hospitalized in Poland. Environ. Pollut. 306, 119469. https://doi.org/10.1016/j.envpol.2022.119469.

Sahihi, M., Faraudo, J., 2022a. Molecular dynamics simulations of adsorption of SARS-CoV-2 spike protein on polystyrene surface. J. Chem. Inf. Model. 62, 3814–3824. https://doi.org/10.1021/acs.jcim.2c00562.

Sahihi, M., Faraudo, J., 2022b. Computer simulation of the interaction between SARS-CoV-2 spike protein and the surface of coinage metals. Langmuir. 38, 14673–14685. https://doi.org/10.1021/acs.langmuir.2c02120.

Sanità di Toppi, L., Sanità di Toppi, L., Bellini, E., 2020. Novel coronavirus: how atmospheric particulate affects our environment and health. Challenges 11, 6. https://doi.org/10.3390/challe11010006.

Santurtún, A., Colom, M.L., Fdez-Arroyabe, P., Real, Á. del, Fernández-Olmo, I., Zarrabeitia, M.T., 2022. Exposure to particulate matter: direct and indirect role in the COVID-19 pandemic. Environ. Res. 206, 112261. https://doi.org/10.1016/j.envres.2021.112261.

Setti, L., Passarini, F., De Gennaro, G., Barbieri, P., Pallavicini, A., Ruscio, M., Piscitelli, P., Colao, A., Miani, A., 2020a. Searching for SARS-COV-2 on particulate matter: a possible early Indicator of COVID-19 epidemic recurrence. Int. J. Environ. Res. Public Health 17, 2986. https://doi.org/10.3390/ijerph17092986.

Setti, L., Passarini, F., De Gennaro, G., Barbieri, P., Perrone, M.G., Borelli, M., Palmisani, J., Di Gilio, A., Piscitelli, P., Miani, A., 2020b. Airborne transmission route of COVID-19: why 2 meters/6 feet of inter-personal distance could not be enough. Int. J. Environ. Res. Public Health 17, 2932. https://doi.org/10.3390/ijerph17082932.

Setti, L., Passarini, F., De Gennaro, G., Barbieri, P., Perrone, M.G., Borelli, M., Palmisani, J., Di Gilio, A., Torboli, V., Fontana, F., Clemente, L., Pallavicini, A., Ruscio, M., Piscitelli, P., Miani, A., 2020c. SARS-Cov-2RNA found on particulate matter of Bergamo in northern Italy: first evidence. Environ. Res. 188, 109754. https://doi.org/10.1016/j.envres.2020.109754.

Setti, L., Passarini, F., Gennaro, G.D., Barbieri, P., Licen, S., Perrone, M.G., Piazzalunga, A., Borelli, M., Palmisani, J., Gilio, A.D., Rizzo, E., Colao, A., Piscitelli, P., Miani, A., 2020d. Potential role of particulate matter in the spreading of COVID-19 in northern Italy: first observational study based on initial epidemic diffusion. BMJ Open 10, e039338. https://doi.org/10.1136/bmjopen-2020-039338.

Shao, L., Ge, S., Jones, T., Santosh, M., Silva, L.F.O., Cao, Y., Oliveira, M.L.S., Zhang, M., BéruBé, K., 2021. The role of airborne particles and environmental considerations in the transmission of SARS-CoV-2. Geosci. Front. 12, 101189. https://doi.org/10.1016/j.gsf.2021.101189.

Tang, S., Mao, Y., Jones, R.M., Tan, Q., Ji, J.S., Li, N., Shen, J., Lv, Y., Pan, L., Ding, P., Wang, X., Wang, Y., MacIntyre, C.R., Shi, X., 2020. Aerosol transmission of SARS-CoV-2? Evidence, prevention and control. Environ. Int. 144, 106039. https://doi.org/10.1016/j.envint.2020.106039.

Tositti, L., Brattich, E., Masiol, M., Baldacci, D., Ceccato, D., Parmeggiani, S., Stracquadanio, M., Zappoli, S., 2014. Source apportionment of particulate matter in a large city of southeastern Po Valley (Bologna, Italy). Environ. Sci. Pollut. Res. Int. 21, 872–890. https://doi.org/10.1007/s11356-013-1911-7.

Tung, N.T., Cheng, P.-C., Chi, K.-H., Hsiao, T.-C., Jones, T., BéruBé, K., Ho, K.-F., Chuang, H.-C., 2021. Particulate matter and SARS-CoV-2: a possible model of COVID-19 transmission. Sci. Total Environ. 750, 141532. https://doi.org/10.1016/j.scitotenv.2020.141532.

Turoňová, B., Sikora, M., Schürmann, C., Hagen, W.J.H., Welsch, S., Blanc, F.E.C., von Bülow, S., Gecht, M., Bagola, K., Hörner, C., van Zandbergen, G., Landry, J., de Azevedo, N.T.D., Mosalaganti, S., Schwarz, A., Covino, R., Mühlebach, M.D., Hummer, G., Krijnse Locker, J., Beck, M., 2020. In situ structural analysis of SARS-CoV-2 spike reveals flexibility mediated by three hinges. Science. 370, 203–208. https://doi.org/10.1126/science.abd5223.

Twigg, B.M.V., Phillips, P.R., 2009. Cleaning the air we breathe - controlling diesel particulate emissions from passenger cars. Platin. Met. Rev. 53, 27–34. https://doi.org/10.1595/147106709X390977.

Vanommeslaeghe, K., Hatcher, E., Acharya, C., Kundu, S., Zhong, S., Shim, J., Darian, E., Guvench, O., Lopes, P., Vorobyov, I., MacKerell, A.D., 2010. CHARMM general force field (CGenFF): a force field for drug-like molecules compatible with the CHARMM all-atom additive biological force fields. J. Comput. Chem. 31, 671–690. https://doi.org/10.1002/jcc.21367.

Vardanega, D., Picaud, S., 2014. Water and formic acid aggregates: a molecular dynamics study. J. Chem. Phys. 141, 104701. https://doi.org/10.1063/1.4894658.

Walls, A.C., Park, Y.J., Tortorici, M.A., Wall, A., McGuire, A.T., Veesler, D., 2020. Structure, function, and antigenicity of the SARS-CoV-2 spike glycoprotein. Cell. 181 (281–292), e1–e6. https://doi.org/10.1016/j.cell.2020.02.058.

Wang, B., Chen, H., Chan, Y.L., Oliver, B.G., 2020. Is there an association between the level of ambient air pollution and COVID-19? Am. J. Phys. Lung Cell. Mol. Phys. 319, L416–L421. https://doi.org/10.1152/ajplung.00244.2020.

Wang, J., Yu, Y., Leng, T., Li, Y., Lee, S.-T., 2022. The inhibition of SARS-CoV-2 3CL Mpro by graphene and its derivatives from molecular dynamics simulations. ACS Appl. Mater. Interfaces 14, 191–200. https://doi.org/10.1021/acsami.1c18104.

Woo, H., Park, S.-J., Choi, Y.K., Park, T., Tanveer, M., Cao, Y., Kern, N.R., Lee, J., Yeom, M.S., Croll, T.I., Seok, C., Im, W., 2020. Developing a fully glycosylated full-length SARS-CoV-2 spike protein model in a viral membrane. J. Phys. Chem. B 124, 7128–7137. https://doi.org/10.1021/acs.jpcb.0c04553.

Yao, H., Song, Y., Chen, Y., Wu, N., Xu, J., Sun, C., Zhang, J., Weng, T., Zhang, Z., Wu, Z., Cheng, L., Shi, D., Lu, X., Lei, J., Crispin, M., Shi, Y., Li, L., Li, S., 2020. Molecular architecture of the SARS-CoV-2 virus. Cell. 183, 730–738. https://doi.org/10.1016/j.cell.2020.09.018.

Zoran, M.A., Savastru, R.S., Savastru, D.M., Tautan, M.N., 2020. Assessing the relationship between surface levels of PM2.5 and PM10 particulate matter impact on COVID-19 in Milan, Italy. Sci. Total Environ. 738, 139825. https://doi.org/10.1016/j.scitotenv.2020.139825.